[UCI]I804:24011-200000267085

February 2019
Thesis for Doctoral Degree

The Role of Autophagy in Plant Defense Response during Phytopathogen Infection

Graduate School of Chosun University

Department of Life Science

Beomgi Lee

The Role of Autophagy in Plant Defense Response during Phytopathogen Infection

식물 방어 반응에서 autophagy의 주요 역할

February 25, 2019

Graduate School of Chosun University

Department of Life Science

Beomgi Lee

The Role of Autophagy in Plant Defense Response during Phytopathogen Infection

Supervised by Professor Hyeonsook Cheong

A thesis submitted to the Graduate School of the Chosun University in partial fulfillment of the requirements for the Doctor of Philosophy

October 2018

Graduate School of Chosun University

Department of Life Science

Beomgi Lee

Beomgi Lee's doctoral thesis has approved by

Chairman: Soo Young Kim, Ph.D _____

Committee Members: Yoonkyung Park, Ph.D _____

Young Soon Kim, Ph.D _____

Indeok Hwang, Ph.D _____

Hyeonsook Cheong, Ph.D _____

December 2018

Graduate School of Chosun University

CONTENTS

CHAPTER 2.

Functional implication of autophagy in pepper fruits infected with anthracnose fungus

LIST OF TABLES AND FIGURES

ABBREVIATIONS

2-ME	**2-mercaptoethanol**
APX	**Ascorbate peroxidase**
DDSA	**Dodecenylsuccinic anhydride**
DMP-30	**2,4,6-Tris(dimethylaminomethyl)phenol**
DPI	**Day post-inoculation**
DTT	**Dithiothreitol**
ECL	**Enhanced chemiluminescence**
EDTA	**Ethylenediaminetetraacetic acid**
ELISA	**Enzyme-linked immunosorbent assay**
GEB	**General extract buffer**
HPI	**Hours post-inoculation**
LM	**Light microscopy**
NMA	**Nadic methyl anhydride**
OsO_4	**Osmium tetroxide**
PBS-T	**Phophate buffered saline with Tween-20**
PMSF	**Penylmethanesulfonyl fluoride**
PVDF	**Polyvinylidene fluoride membrane**
ROS	**Reactive oxygen species**
RT-PCR	**Reverse-transcriptase PCR**
SDS	**Sodium dodecyl sulfate**

SDS-PAGE	**SDS-polyacrylamide gel electrophoresis**
SOD	**Superoxide dismutase**
TBS-T	**Tris-buffered saline with Tween-20**
TEM	**Transmission electron microscopy**

초 록

식물 방어 반응에서 autophagy의 주요 역할

이 범 기

지도교수 : Prof. 정현숙, Ph.D

조선대학교 대학원

생명과학과

Autophagy는 식물에서 병원체의 침임에 대항하기 위한 면역적 방어기작에 필수적으로 요구된다. 병원체 침입 시, 식물은 즉각적으로 autophagy, apoptosis, necrosis와 같은 면역 기작을 작동시켜 세포내로 병원체의 감염이 이뤄지는 것을 막는다. 그러나 병원체 또한 그들의 생존에 필요한 기작들을 활성화 시켜 식물 방어 체계를 회피하여 살아남는다. 많은 과학자들은 병원체와 식물체 간의 autophagy와 같은 면역적 상호연관관계를 밝히고자 노력해왔다. 그 결과, 많은 부분에 대해서 궁금증을 해결 할 수 있었지만, 아직 일부 병원체와의 연관관계를 밝히지는 못하였다.

본 연구는 potato virus Y-O(PVY^{O})와 *Nicotiana benthamiana*, *Colletotrichum*

gloeosporioides (*C. gloeosporioides*)와 고추 열매와의 상호연관관계를 입증했다. PVY^{O}와 *N. benthamiana*와의 상호연관관계를 밝히기 위해서 *N. benthamiana*에 직접 PVY^{O}를 감염시켜 형태학적 분자생물학적 분석을 진행하였다. 형태학적 분석을 위해서 4 주차의 식물에 PVY^{O}를 감염을 시킨 후 시간 별 사진을 비롯하여 잎의 길이 측정, 병징 관찰, ELISA를 이용한 virus 입자의 생성 관찰, transmission electron microscope(TEM)와 light microscope(LM)를 이용하여 병징이 나타난 잎에서의 virus 분포도 관찰을 시행하였다. 분자생물학적 분석은 PVY^{O} 감염 후에 잎의 위치에 따라 RT-PCR과 western blot을 통하여 RNA와 protein level에서의 변화를 관찰하였다.

*C. gloeosporioides*는 appressorium이라 불리는 자신의 미세기관을 이용하여 고추 열매에 부착하고 침입한다. 고추에 부착 후 침입이 이루어질 때, 고추는 병원체의 침입과 확산을 막기 위해 autophagy과 같은 다양한 방어기작을 일으킨다. 본 연구에서는 *C. gloeosporioides*를 감염 시켰을 때 fungi와 고추열매를 염색하여 *C. gloeosporioides*의 appressorium 형태와 부착, 침입을 관찰하였다. 또한, wetern blot을 이용하여 *C. gloeosporioides*의 침입에 따른 분자생물학적 변화를 관찰하였다. 그 결과 *C. gloeosporioides* 감염 후에 시간이 지남에 따라 autophagy 관련 protein들의 level이 증가하였고 이와 연관된 방어 protein들의 level 또한 증가함을 확인 할 수 있었다.

결론적으로, PVY^{O}또는 *C. gloeosporioides*가 식물에 감염이 되면 식물체의 방어기작을 유도한다. 여러 가지 방어기작 중, 병원체가 감염되었을 때 빠른 시간 내에 autophagy가 작동하여 식물체 내로 병원체가 확산되는 것을 방어한다. 이 실험에서는 autophagosome을 형성하는데 기여하는 ATG4, ATG8을 확인하였고, 병원체 침입 시 발생하는 ROS 제거를 위해 발생하는 여러가지 antioxidant enzyme의 발현을 확인하였다. 또한 pathogen 침입 시 발현되는 pathogen related protein을 확인하였다. Virus의 경우 virus genomic RNA를 silencing 시키기 위하

여 small interfering RNA (siRNA)를 만든다. 이 과정에 있는 dicer like protein (DCL)과 argonaute (AGO)의 발현량을 확인하였다. 그 결과 virus의 감염시 시간이 지남에 따라 DCL과 AGO의 전사 level이 감소됨을 확인하였다. 이는 virus의 구성 요성 중 RNA silencing을 방해하는 요소가 있음을 암시한다.

GENERAL ABSTRACT

The Role of Autophagy in Plant Defense Response during Phytopathogen Infection

Beomgi Lee

Advisor : Prof. Hyeonsook Cheong, Ph.D.

Department of Life Science,

Graduate School of Chosun University

Autophagy is essentially required for immune defense against pathogens attack in plants. When a pathogen infects, plants immediately initiate a variety of their defense mechanisms, such as autophagy, apoptosis and necrosis, to block spreading of pathogenic components into cells. But pathogens activate their own survival mechanisms to avoid the plant defense mechanisms. So, many researchers have tried to investigate the interrelation between pathogens and plants.

I tried to investigate the correlation of *potato virus* Y-O (PVY^O) with *Nicotiana benthamiana* and *Colletotrichum gloeosporioides* (*C. gloeosporioides*) with pepper fruits, respectively. To study correlations brtween PVY^O and *N. benthamiana*, I

performed morphological and molecular biological analysis after direct virus infection on the plant. For morphological analysis, 4 weeks old *N. benthamiana* plants inoculated with PVY^{O}, was employed to carry out measurement of leaf length, observation of symptoms, quantification of virus particles according to leaf position using ELISA and observation of virus distribution on diseased leaves using light microscopy and transmission electron microscopy, etc. For molecular biological analysis, RNA or protein expression levels, according to the position of leaves after PVY^{O} infection were examined using RT-PCR and western blot. In tobacco (*N. benthamiana*), infection of mild strain of PVY^{O} induced stunted growth in young leaves and then mosaic symptom begun to appear on top leaf at 13 dpi. To investigate whether the mild symptom development was associated with defense reaction against virus, general defense reactions were systemically analyzed in infected plants in association with autophagy pathway. Overall, our results indicate that autophagy may play a role in the suppression of virus symptom development in non-host tobacco plants during early response to PVY^{O} infection.

C. gloeosporioides is the causal agent of anthracnose in hot pepper fruits and adopts a hemibiotrophic lifestyle. Its initial biotrophic phase involves a series of infection processes and followed by a necrotrophic stage. To defend against the hemi-biotrophic anthracnose fungus, the plant may need to provoke complex defense reactions to attenuate fungal virulence. In our system, the infected green fruits showed hypersensitive reaction (HR) that resulted in lesion formation during the necrotrophic phase. I observed ROS formation, the accumulation of antioxidant proteins and autophagy-related proteins in association of fungal infection. Autophagy was shown to be induced by the invasion of fungus; autophagy-related protein levels that were accompanied with the induction of defense-related proteins

representing differential expression patterns between compatible green fruits and incompatible red fruits. Tentative physiological roles of autophagy was discussed in the pepper fruits during phytopathogen interaction.

In conclusion, PVY^{O} or *C. gloeosporioides* infection triggered defense mechanisms in their host plants. Among the defensive mechanisms, autophagy was activated in a short time during pathogen infection, preventing pathogens from spreading. Futhermore, endoplasmic reticulum (ER) stress may induce two cell defence pathways, the unfolded protein response (UPR) or programmed cell death (PCD) upon biotic stress. In our experimental systems, promoted up-regulation of UPR genes in *N. benthamiana* increased resistance to potato virus Y (PVY^{O}) by enhancing autophagy pathway that plays a role in the process of viral infection. On the contrary, the ER stess and autophagy that were activated during fruit development of hot pepper fruits proceeded further a programmed cell death in infected cells upon fungal infection. Thus, autophagy represents a anti-pathogenic mechanism that plays an important role in antiviral immunity in tobacco and in antifungal reaction in red pepper fruits, respectively.

CHAPTER 1

The Role of autophagy during phytopathogen interaction between *N. benthamiana* and potato virus Y (PVY^O)

1.1 ABSTRACT

Potato virus Y (PVY) is an aphid-transmitted Potyvirus that affects economically important solanaceous species including potato, tobacco, tomato, and pepper. In this study, the phenomena following infection with Potato virus Y was investigated in tobacco (*Nicotiana benthamiana*). In tobacco plants, infection of mild strain of PVY (PVY^O) induced stunted growth in the first two leaves at the shoot apex starting 7 days post-infection (dpi) and then mosaic symptom began to appear on newly developing young leaves at 13 dpi. Enzyme-linked immunosorbent assays revealed that the virus particles were highly accumulated in developing leaves in the upper part of infected plants. To investigate whether delayed symptom development in the leaves were associated with defense reaction against the virus, the leaves from base to top of the plants were analyzed for ROS generation. Rapid and prolonged accumulation of superoxide (O_2-) and hydrogen peroxide (H_2O_2) was detected in the young leaves from the first day of infection, following

increase of ROS-scavenging enzymes such as superoxide dismutases, ascorbate peroxidases, and catalase. Furthermore, the oxidative defense was associated with the induction of autophagy markers, ATG4 and ATG8, respectively. Cleavage of ATG8 was induced in upper part of infected plants, indicating a physiological role of virus induced autophagy in the plant. Additionally, pathogenesis-related protein3 (PR3) was also increased during defense reaction of the plants against the virus. Overall, our results indicate that autophagy may play a role in the suppression of virus symptom development in non-host tobacco plants during early response to PVY^{O} infection.

1.2 INTRODUCTION

Potato (*Solanum tuberosum L.*) is one of the important vegetable crops belongs to the *Solanaceae* family (Kassim, 2014). Potatoes (*Solanum tuberosum L.*) are the fourth most consumed food crop grown worldwide and were valued at $6 billion globally in 2005 (FAO, 2008). Potatoes are vegetatively propagated and pathogens, including viruses, spread more readily to progeny compared to crops that are propagated from true seeds (Karasev, 2013). Potato seed certification laboratories and growers utilize several measures including tissue culture propagation, field inspection, and diagnostic testing to ensure pathogen-free seed potato stock. Pathogen transmission and disease are reduced by extensive pathogen monitoring programs and by limiting the number of field-grown generations.

PVY has a broad host range in nature and can infect 14 genera plants of *Solanaaceae*. (Kerlan, 2006, Ximba, 2017, Fulladolsa, 2018). More than 50 aphids can infect PVY in a non-persistent manner. Symptoms of infected plants include mosaic symptoms, leaf drop, leaf crinkle, leaf chlorosis, leaf necrosis, cracking and necrotic ring on tubers (Radcliffe, 2002). PVY is a single-stranded, positive-sense RNA genome of 9·7 kb (Karasev & Gray, 2013). It was recently ranked as the fifth most important plant virus worldwide (Scholthof, 2011). Globally, it causes the most important virus disease of potato (*Solanum tuberosum*). PVY induces major losses in potato tuber yield and diminishes quality by causing potato tuber necrotic ring-spot disease (PTNRD) (Valkonen, 2007, Gray, 2010, Karasev 2013, Jones, 2014). It also causes severe diseases in other important *solanaceous* crops, including tobacco (*Nicotiana tabacum*), tomato (*Solanum lycopersicum*) and pepper (*Capsicum annuum*) (Kerlan, 2006, Blanchard, 2008, Kerlan, 2008).

Excessive ROS may cause irreversible oxidative damage to proteins, lipids, and nucleic acids and activate signaling pathways ultimately leading to cell death (Apel, 2004). However, at low levels, ROS participate in pro-survival mechanisms, acting as second messengers that transmit initial stress signals allowing cells to react and adapt to different environmental cues (Mittler, 2011). The chloroplast is known to be one of the main sources of ROS in plants and algae. Superoxide anions ($O2^-$) are generated as by-products of photosynthetic electron transport and readily converted into hydrogen peroxide (H_2O_2) inside the chloroplast through chemical and enzymatic reactions. Singlet oxygen ($^1O_2$) and hydroxyl radicals are also produced during photosynthesis and can cause oxidative damage. In addition to the chloroplast, ROS are produced in plant cells in mitochondria, peroxisomes, and at the plasma membrane by NADPH oxidases. H_2O_2 is recognized as an important signaling molecule in a wide range of organisms, including plants. H_2O_2 regulates numerous processes such as cell division, differentiation, and growth as well as apoptosis and plays a major role in the control of plant development and adaptation to biotic and abiotic stresses (Foyer, 2009). Recent studies in photosynthetic organisms described the activation of autophagy in response to several stimuli that increase ROS generation, regardless of the origin and location of ROS production in the cell (Xiong, 2007, Liu, 2009, Pérez-Pérez, 2010, 2012).

The intracellular physiological responses of plants to adverse environmental conditions is critical for their survival. A key process by which plant cells respond to environmental stresses is vacuolar autophagy (Greek for self-eating), whereby cytoplasmic components are degraded in the vacuole to provide raw materials and energy, and also to eliminate damaged or toxic components, for the maintenance of essential cellular functions. During autophagy, cytoplasmic components are

nonselectively enclosed within a double-membrane vesicle known as the autophagosome and delivered to the vacuole/lysosome for degradation of toxic components and recycling of needed nutrients (He and Klionsky, 2009, Mizushima , 2011, Liu and Bassham, 2012). This degradative process is widely conserved through evolution, and accordingly, autophagy-related (ATG) genes have been found in all eukaryotes (Tsukada and Ohsumi, 1993) The ATG5-ATG12-ATG16 protein complex and the ATG8-phosphatidylethanolamine (PE) conjugate are essential for autophagosome formation and completion, while ATG8-PE also mediates fusion of the autophagosome to the vacuole membrane (Mizushima, 2011). The ATG4 Cystein protease processes nascent ATG8 at the C terminus to facilitate its covalent binding to PE, but it is also able to cleave PE from ATG8 for its recycling, playing a crucial role in autophagy regulation (Kirisako, 2000).

A viral RNA induces specific plant defence responses in which a large number of plant proteins participate; among them, dicer-type dsRNA RNases, ssRNA RNases belonging to the Argonaute-type protein family, which assemble in RNA-induced silencing complexes (RISC), RNA polymerases and RNA helicases (Dunoyer and Voinnet, 2005). This antiviral response, which is one of the manifestations of a complex set of cellular processes known as RNA silencing, is apparently universal; so for the virus to be successful it has to escape it. Although viruses may adopt various strategies to go about achieving this, it is believed the most usual strategy they adopt is that of producing silencing suppressors (Li and Ding, 2006, Valli, 2009). These suppressors not only affect antiviral defence, but also interfere with plant physiological processes that depend on RNA silencing, and this interference may contribute significantly to the pathogenesis of different viruses (Vicente and Juan, 2011).

Many scientists are studying virus resistant plants. However, the role of autophagy due to viral infection has not been fully understood yet. I carried out a study on the virus resistance mechanism of autophagy after PVY infection. I also studied plant defense mechanisms related to autophagy before the onset of symptoms. This study was conducted to investigate the resistance mechanism of plants when plants were infected with PVY.

1.3 MATERIALS AND METHODS

1.3.1 Plant materials and growth conditions

All experiments were performed with tobacco (*Nicotiana benthamiana*). The seeds were germinated in pots containing autoclaved culture soil. Five days old seedlings after germination were transferred to round pots. Plants were grown at 24 ± 2 ˚C in a growth room with a 16 hours light / 8 hours dark photoperiod. Four weeks old plants were used in PVY^{O} inoculation.

1.3.2 PVY^{O} inoculation and sample collection

Potato Y^{O} virus (PV-575) was obtained from the American Type Culture Collection (ATCC). The virus inoculum were prepared by grinding 100 mg PVY^{O}-infected leaves in 3 mL of 50 mM potassium phosphate buffer, pH 7.5 with 100 mg silicon carbide. Four weeks old tobacco plants, when the fifth leaves come out, were inoculated onto tobacco leaves by mechanical method using a cotton swab. inoculated PVY^{O}. After inoculation, tobacco plants were incubated in humid box in dark condition for overnight. Non-inoculated tobacco plants also were incubated under the same conditions. The leaves of PVY^{O} inoculated plant were collected at 0, 3, 7, 9, 11, 14, 21 days post-inoculation (DPI). All samples were immediately frozen in liquid nitrogen and stored at −70 ˚C.

1.3.3 Measurement of leaf length

The leaf length was measured from petiole end to leaf end using a ruler. The leaf length was compared using the 6th leaf after 4 DPI between control and inoculated plants.

1.3.4 Enzyme-linked immunosorbent assay (ELISA)

To measure the amount of virus particles, a double sandwich ELISA (Agdia, Inc., Elkhart, IN, USA) was used according to the manufacturer's instructions. Briefly, the inoculated samples were ground with Agdia's general extract buffer (GEB) at a 1:10 ratio (FWg/mL), and 100 μL of the prepared extracts was applied to anti-PVY^{O} coated micro-plate and incubated for overnight in the refrigerator (4 ˚C). The well washed several times with phosphate buffered saline containing Tween-20 (PBS-T) and added 100 μL enzyme-conjugates into the each well. After 2 hours incubation at room temperature in the dark, the well was washed with PBS-T, and *p*-nitro phenyl phosphate was added to each well. The absorbance was measured at 405 nm using UV-spectrophotometer (Biotek, winooski, VT, USA).

1.3.5 RNA extraction, cDNA synthesis and reverse-transcriptase PCR (RT-PCR)

On the 11 and 14 DPI after PVY^{O} inoculation, the RNA were extracted from the upper 3rd, 7th, and 9th leaves of inoculated plants. For the RNA extraction, The leaves were ground using a mortar with liquid nitrogen. 1 mL of RNA extract solution (Hybrid-R^{TM}, Geneall, Korea) was added per 100 mg according to the

manufacturer's instructions. The purified RNA was quantified using a UV-spectrophotometer and 2 μg of RNA was converted to cDNA using reverse transcriptase (Hyperscript™, GeneAll). The expression of autophagy related genes and other genes were confirmed by RT-PCR using specific primers. The RT-PCR was performed with a thermocycler (PTC-200, Bio-Rad, Hercules, CA, USA) using the following PCR conditions: 30 cycles of 95 ˚C for 30 sec, 60 ˚C for 30 sec and 72 ˚C for 30 sec. PCR products were separated in 1% agarose gel containing ethidium bromide (EtBr). Primer sequences are shown in Table 1.1.

1.3.6 Immunoblot analysis

The frozen leaf tissues were ground using mortar with liquid nitrogen. The lysate was resuspended in 2 volumes lysis buffer (consisted of 50 mM sodium phophate (pH 7), 10 mM EDTA (ethylenediaminetetraacetic acid, pH 8), 10 mM 2-ME (2-mercaptoethanol), 4 mM DTT (dithiothreitol), 0.1% triton X-100, 0.1% SDS (sodium dodecyl sulfate), 200 μM PMSF (phenylmethanesulfonyl fluoride), 250 mM sucrose, 10% glycerol and protein inhibitor cocktail (Sigmal Aldrich). The lysates were shaking incubated in refrigerator (4 ˚C) for 2 hours and then centrifuged at 4 ˚C. The supernatant of extracted protein was quantitated using Bradford assay to determine the amount of protein. The protein samples (20 μg) were heated at 100 ˚C for 10 min, separated in 12% SDS-PAGE (SDS-polyacrylamide gel electrophoresis) at 100 voltage for 90 mins at room temperature and transferred onto a polyvinylidene fluoride membrane (PVDF, 0.45 μm pore size, immobilon-FL, Merck Millipore Ltd.) for 90 mins at 4 ˚C. The membranes were blocked with 5% skim milk in TBS-T (tris-buffered saline with

Tween-20) buffer for 1 hour on the shaking incubator at room temperature. The washing step was always repeated 3 times for 10 mins with TBS-T buffer. Primary antibody was added to membrane and shaking incubated overnight at 4 ° C. After washing with TBS-T, the membranes were incubated with secondary antibody conjugated with peroxidase at room temperature according to the specificity of primary antibody. The blots combined with primary and secondary antibody were detected using the enhanced chemiluminescence (ECL) plus detection reagents (Claro sola, BioD Co., Ltd., Korea). Antibody informations are shown in Table 1.3.

1.3.7 Light microscopy (LM) and transmission electron microscopy (TEM)

1.3.7.1 Leaves collection for LM and TEM

For transmission light microscopy and electron microscopy, the upper 8th and 10th leaves were harvested from the inoculated plants in 9 and 13 DPI with control plants. The control and inoculated plants were cut (1×2 mm^2 for EPON embedding and 3×3 mm^2 for paraffin embedding) and fixed in 4% para-formaldehyde in 50 mM sodium phosphate buffer at pH 7.0.

1.3.7.2 Light microscopy (LM) analysis for immunohistochemistry

The fixed specimens were dehydrated using ethanol. For dehydration, the specimens passed through the following series; (1) 30－70% ethanol for 25 mins

in ice on shaker; (2) 80－100% ethanol for 25 mins at room temperature on shaker; (3) Next, 1:1 ethanol and chloroform; (4) 100% chloroform; (5) 1:1 chloroform and paraffin; (6) 100% paraffin mixture for 30 mins, respectively. Steps (1) to (5) were performed at room temperature, and steps (5) and (6) were performed at 65 ˚C. After overnight incubation at 65 ˚C, samples were transferred to mold for solidification. The paraffin blocks were cut into 5 μm thicknesses and attached on the slide glass at 40 ˚C. The completed samples were used for immunohistochemistry (IHC).

1.3.7.3 Transmission electron microscopy (TEM) analysis

To observe ultrastructure of plant tissue, the aldehyde-fixed specimens were post-fixed in 1% osmium tetroxide (OsO_4) in 100 mM sodium phosphate buffer (pH 7.0) for 2 hours on ice. Then the samples were washed 5 times with 100 mM sodium phosphate buffer. The fixed specimens were passed through increasing concentrations of ethanol (30, 50, 70, 90 and 100%) for 15 min, respectively. Dehydrated segments were infiltrated with 100% propylene oxide (15 mins, 2 times), 2:1 propylene oxide with epon mixture (50 mins), 1:1 propylene oxide with epon mixture (50 mins), 1:2 propylene oxide with epon mixture (50 mins), and then put the samples in 100% epon mixture (for overnight at shaking). The epon mixtures consisted of epoxy EM bed-812 24 g, DDSA 9 g and NMA 15 g (Electron microscopy sciences inc., Hatfield, PA, USA). Epon embedding was performed using epon mixture with DMP-30 0.5 g. The mold was then incubated on root temperature for overnight and then incubated for 1 day at 60 ˚C. The epon samples were cut into series of semi-thin (1 μm thick) and thin section (100

nm thick). Series of semi-thin section pieces were put on a slide glass and stained with 1% toluidine blue. The thin section pieces onto the grid and stained with 4% uranyl acetate.

1.3.8 Constructions of autophagy-related genes and production of transgenic plants

For the isolation of *ATG5* and *ATG8* genes in *N. benthamiana*, the genes of *Arabidopsis* were searched on the website (TAIR, https://www.arabidopsis.org). Based on the sequences, the homologous loci were investigated in National Center for Biotechnology Information (NCBI, https://www.ncbi.nlm.nih.gov) and Sol genomics network (https://solgenomics.net). For the isolation of *ATG5* and *ATG8f* from *N. benthamiana*, total RNA was isolated from healthy tobacco leaves. Total RNA was converted to cDNA using oligo d(T). *ATG5* and *ATG8f* were identified using gene specific primers. The identified *ATG5* and *ATG8f* cDNAs were cloned using an In-fusion system (Takara, Japan). *ATG5* was inserted into the pPZP212-p35S::eYFP vector, and *ATG8f* was inserted into the pBI121-pCsVMV::eGFP vector (Fig 1.18.). Each cloned vector was transformed into *Escherichia coli* DH5α strain and selected by selection marker (pPZP212-eYFP was selected using spectinomycin and pBI121 was selected using kanamycin). The selected right vector was isolated using plasmid prep kit. Purified vectors were transformed into *Agrobacterium tumefaciens* GV3101 strain after sequencing. Positive colony selection was screened using rifamycin, gentamycin and multiple antibiotics of their selection marker. The transformed colonies were used for the transformation of *N. benthamiana*.

1.3.9 Statistical analysis

Statistical analyses were carried out by one-way ANOVA to evaluate whether the means were significantly different using Prism 5.0 software (GraphPad San diego, CA, USA), taking $P < 0.05$ as significance level.

Table. 1.1. *Nicotiana benthamiana* gene-specific primers used in RT-PCR

Gene		Primers (5' to 3')
ATG4	Forward:	GGTGCTCCATTGTTTACGATAAC (20 mers)
	Reverse:	GCAATCAAGTAGAACGACCAGC (22 mers)
ATG5	Forward:	GACCTGTTGAGATTCATGGAGAT (23 mers)
	Reverse:	CTCCAGAATTGCTAATCCTATGAAC (25 mers)
ATG8	Forward:	CTGCTCGGATTAGGGAAAAATAC (23 mers)
	Reverse:	GAACCATAGGCAAATCAACAAACG (24 mers)
AGO1	Forward:	TATGGGAAGGAGCACGCGAG (20 mers)
	Reverse:	AGCCAAGCCAAGGTGTGACA (20 mers)
AGO2	Forward:	TCCAACTTCCACGACCCCAC (20 mers)
	Reverse:	TGCTGTCACCACCACCAAGT (20 mers)
DCL2	Forward:	CGTGAGAATGGCGTGGCGTA (20 mers)
	Reverse:	AGGGCAGAAACCAAAACATACGA (23 mers)
DCL4	Forward:	CTGAGGACGCAGCAGAAGG (19 mers)
	Reverse:	AGACCCCTTTATCACTCCGTACT (23 mers)
Rubisco	Forward:	TCCGGGTATTAGCAAAAGCGT (21 mers)
	Reverse:	TGAAGCCACGGGTAGAACAC (20 mers)

Table. 1.2. PCR primers used for *Nicotiana benthamiana ATG4* and *ATG8* genes construction

Gene		Primers (5' to 3')
NbATG5-YFP	Forward:	CGGGGGACGAGCTCGATGGGAAGTAAAGGGGCAGG (35 mers)
	Reverse:	TGCTCACCATCCCGGATATGGTGATGGGTTCTTGAATTTT (41 mers)
NbATG8-GFP	Forward:	CGCGGGCCCGGGATCATGGCTAAGAGCTCATTCAAGC (37 mers)
	Reverse:	TGGTGGCGATGGATCTCAGCTTGTTCAGGTCCCCG (35 mers)

Table 1.3. Primary antibody informations used in western blot

Antibody name	Manufacturer	Host	Dilution rate
APX	Agrisera	Rabbit	1:2,000
ATG4	Agrisera	Rabbit	1:2,500
ATG8	Agrisera	Rabbit	1:1,000
BiP	Agrisera	Rabbit	1:1,500
CAT	Agrisera	Rabbit	1:2,000
Cu/ZnSOD (CSD2)	Agrisera	Rabbit	1:2,000
FeSOD	Agrisera	Rabbit	1:2,000
LhCa1	Agrisera	Rabbit	1:5,000
LhCa2	Agrisera	Rabbit	1:5,000
LhCb	Agrisera	Rabbit	1:5,000
MnSOD	Agrisera	Rabbit	1:2,000
PR3	Agrisera	Rabbit	1:3,000
PVY-VN	Seoul Women's University	Rabbit	1:2,000

Table 1.4. Secondary antibody informations used in western blot

Antibody name	Manufacturer	Host	Dilution rate
anti-Rabbit	Santacruz biotec.	Goat	1:20,000

1.4 RESULTS

1.4.1 Developmented stage-dependent symptom changes of spreaded virus particles

4-week-oil plants were used for the experiment were grown for 4 weeks old. The plants had 5 leaves (small 6th leaf). The first leaf on the base of plant was mechanically inoculated with PVY^{O} and allowed to stand for 5 mins and washed with distilled water for silicon carbide removal. The plants were then placed in a humid box and stored in a culture room (24 ± 2 ˚C) overnight. The infection rate decreased when the leaves were dry. The plants were given water at 4 to 5 days intervals in the culture room and no water was given before the experiment. Growth of the infected plants was monitored until the end of the plant's lifecycle (data not shown), and the experiment was focused on a short time for the purpose of the experiment (up to 21 days). It was confirmed that the virus spreads rapidly to the upper leaf of the infected plant (Fig 1.1.A). In fact, the virus symptoms appeared on the 13 days post-inoculation (Fig 1.1.B). The symptoms of infection were leaf curl, unstable growth and mosaic symptoms. Especially, the symptoms appeared in newly growing leaves (Fig 1.1.B-b and B-d).

Leaf length was measured from 4 days after inoculation to examine growth retardation in growing leaves. The leaf length was measured from the 6th leaf to the apex using a ruler and the length was measured up to 14 DPI. (Fig 1.2). The length of the leaves that had already grown (6th leaf) was almost same compare to

that of uninfected control. However, it was confirmed that the growth rate of the leaves was inhibited with time compared with control (7^{th} leaves or more). In the 14th day of infection, growth inhibition of leaves was observed in the infected leaves as follows; 4.3% in 6^{th} leaf, 15.7% in 7^{th} leaf, 17.1% in 8^{th} leaf, 25.4% in 9^{th} leaf, 54.5% in 10^{th} leaf, 35.1% in 11^{th} leaf and 36.8% in 12^{th} leaf.

Virus particles were quantified using ELISA in order to confirm the correlation between inhibition of leaf growth and virus. All the leaves were tested for the accumulation of virus particles in the plants on 3, 5, 7, 11, 14, and 21 DPI. Only a small amount of virus particles were detected in the inoculated leaf until the 3 DPI. However, from the 5th day, it was observed that large amount of virus particles were produced in the upper part of the plant. Although the number of leaves increased as the plant grew, virus particles were distributed around the newly formed leaves at the upper part. On 21 DPI, not only virus particles were highly accumulated the upper leaves, but also a small amount of virus particles were detected in the lower leaves of the plant were detected (Fig 1.3).

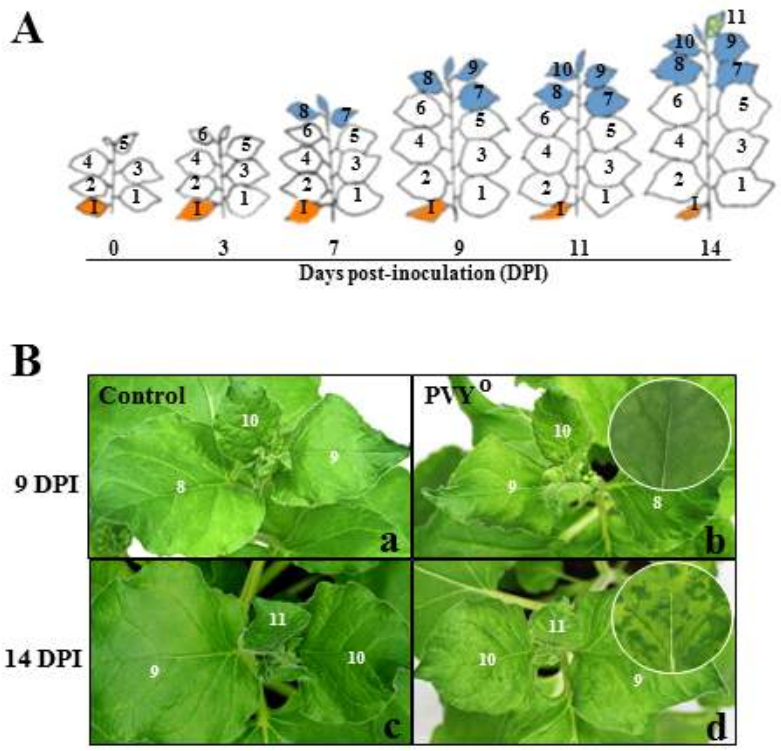

Figure 1.1. Symptom development caused by Potato virus Y-O (PVY^O) in *Nicotiana benthamiana*. **(A)** Developmental stages observed during systemic infection of *N. benthamiana* plants with PVY^O. Control, uninfected 4-weeks old plant; PVY^O, infected plants with PVY^O. Numbers represent the leaf number above the inoculated leaf (I) on the base. Orange indicates inoculated leaves. Blue represent that virus protein is detected in the leaves. Mosaic symptom is illustrated with yellow dots in the leaf. **(B)** Disease symptoms of PVY^O were appeared in a systemic leaf on the top of *N. benthamiana* at 14 days post-infection (dpi). **a**, control plant at 9 dpi; **b**, Infected plant at 9 dpi; **c**, control plant at 14 dpi; **d**, Infected plant at 14 dpi.

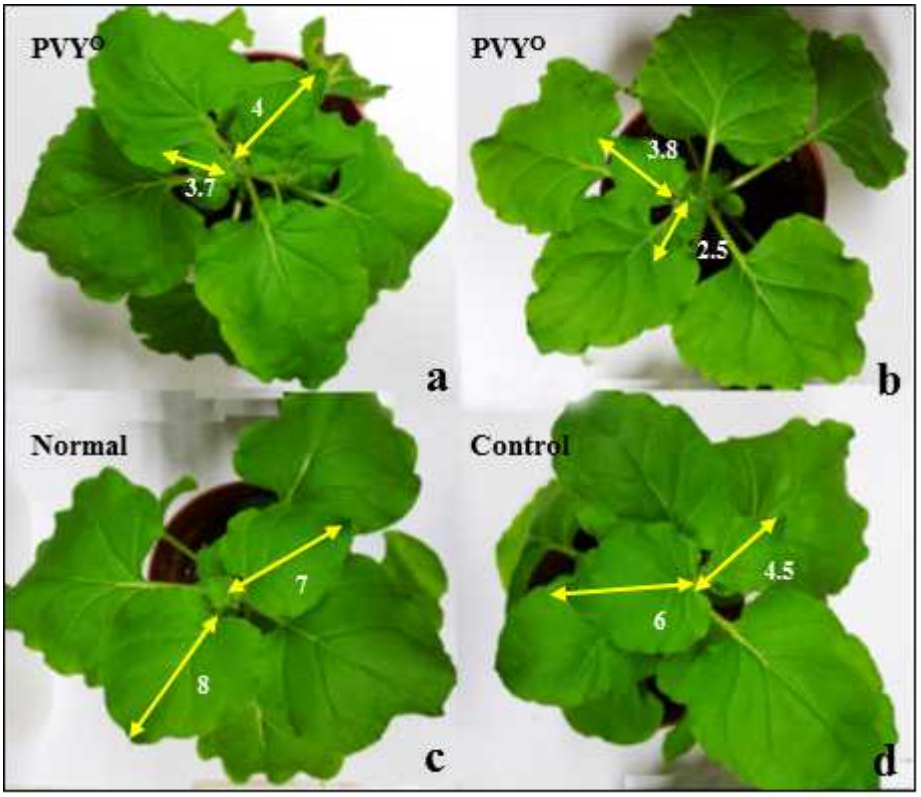

Figure 1.2. Growth retardation in young leaves caused by Potato virus Y-O (PVY^{O}) in *Nicotiana benthamiana*. (A) Leaf size was reduced in young leaves of *N. benthamiana* at 7 days post-infection (dpi) with PVY^{O}. **a**, an infected plant; **b**, an infected plant; **c**, normal plant at same developmental stage; **d**, control plant that was abraded with silicon carbide.

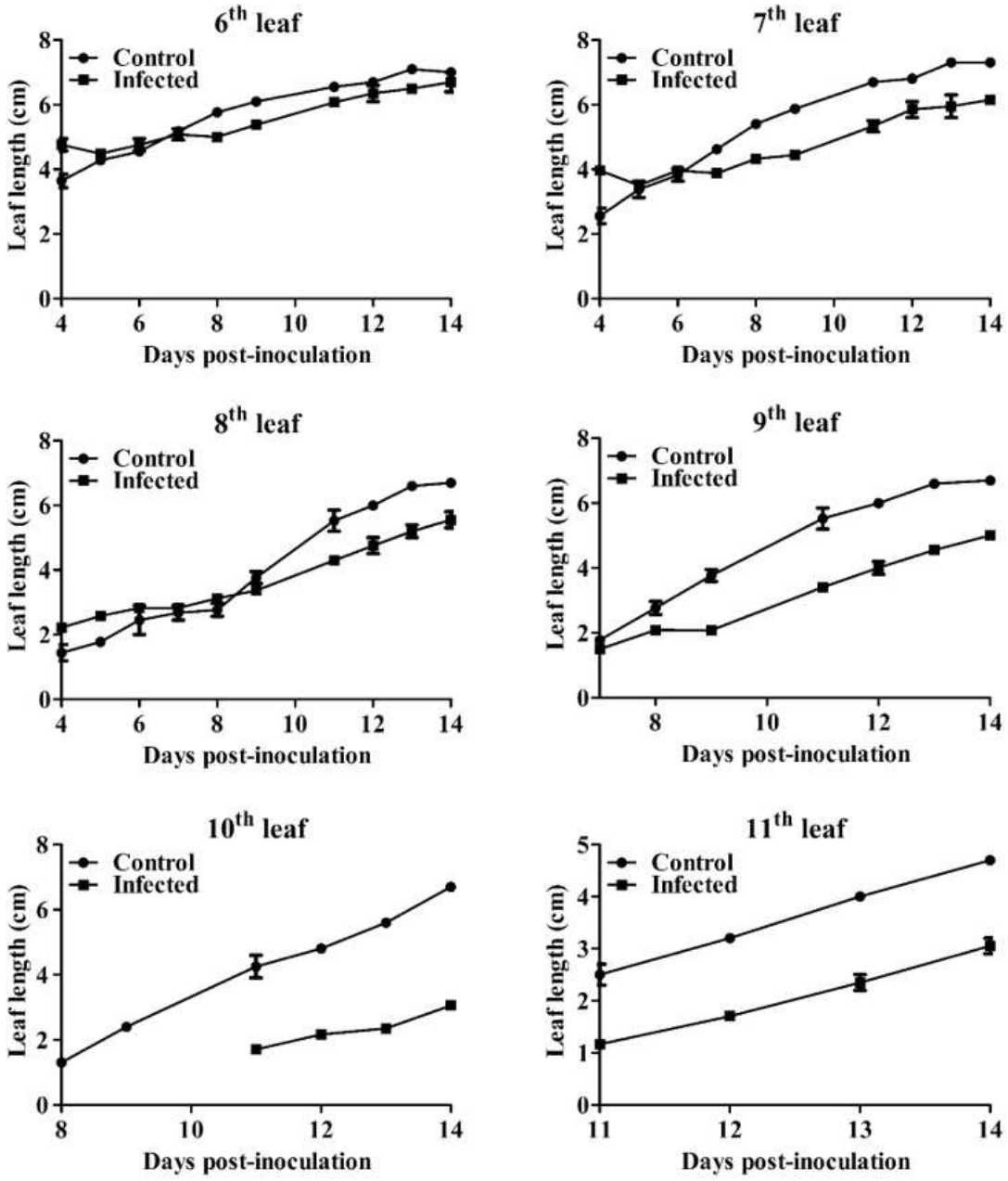

Figure 1.3. Developmental process of leaves after PVY^{O} infection in *Nicotiana benthamiana*. The leaves from 6th to 11th were measured from 4 DPI to 14 DPI. Leaves from infected and normal plants were compared. Each group was measured in 5 individuals.

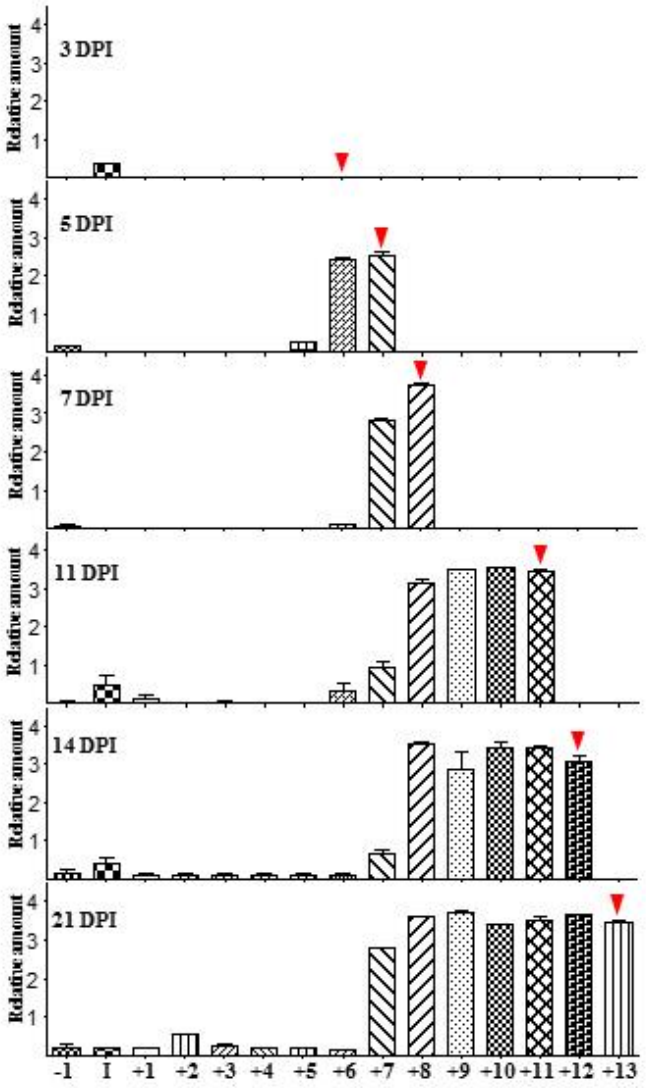

Figure 1.4. Relative amount of virus in the leaves of *Nicotiana benthamiana* infected with PVY^{O}. Virus contents were measured in the leaves of inoculated plants using ELISA. The Y axis indicates ELISA absorbance values. Numbers represent leaf number above the inoculated leaf (I). Rad arrows were displayed location of top leaf at indicated day.

1.4.2 Detection of PVY coat protein using western blot and immunolocalization

The distribution patterns of viruses in infected plants were investigated by visual inspection and ELISA. Then, western blot was performed to confirm the location and amount of virus. Western blot was conducted using total protein from leaves of infected plants on 11, 14 and 21 DPI. Among the components of the virus, coat protein antibody was used to detect virus particles. The rabbit anti-PVY coat protein was diluted 1:2,000 with TBS-T with 0.02% sodium azaide. A large amount of virus coat protein accumulation was observed in the upper part, as in the previous morphological results. The virus coat protein accumulation in the upper leaves was more prominent than virus spreading over time after infection. Especially, virus coat protein was found in newly formed leaves. (Fig 1.4.A).

Next, immunolocalization was performed to observe intercellular localization of virus in the infected plant. The stem of the 14 DPI plant was fixed, dehydrated, infiltrated and embedded in paraffin. The paraffin block was cross-sectioned to a thickness of 5 μm and then rabbit anti-PVY^{O} coat protein was attached. After the addition of goat anti-rabbit IgG conjugated rhodamine red X (Molecular probes, Thermo Fisher Scientific, Inc., USA), fluorescence microscopy was used to identify the position of the virus coat protein in the stem. The viral coat proteins were distributed around the vascular bundles, and were also detected in the outer layer of the cortical cells. The amount of virus was much higher in the 10th stem compare to that in the 8th stem (Fig 1.4.B).

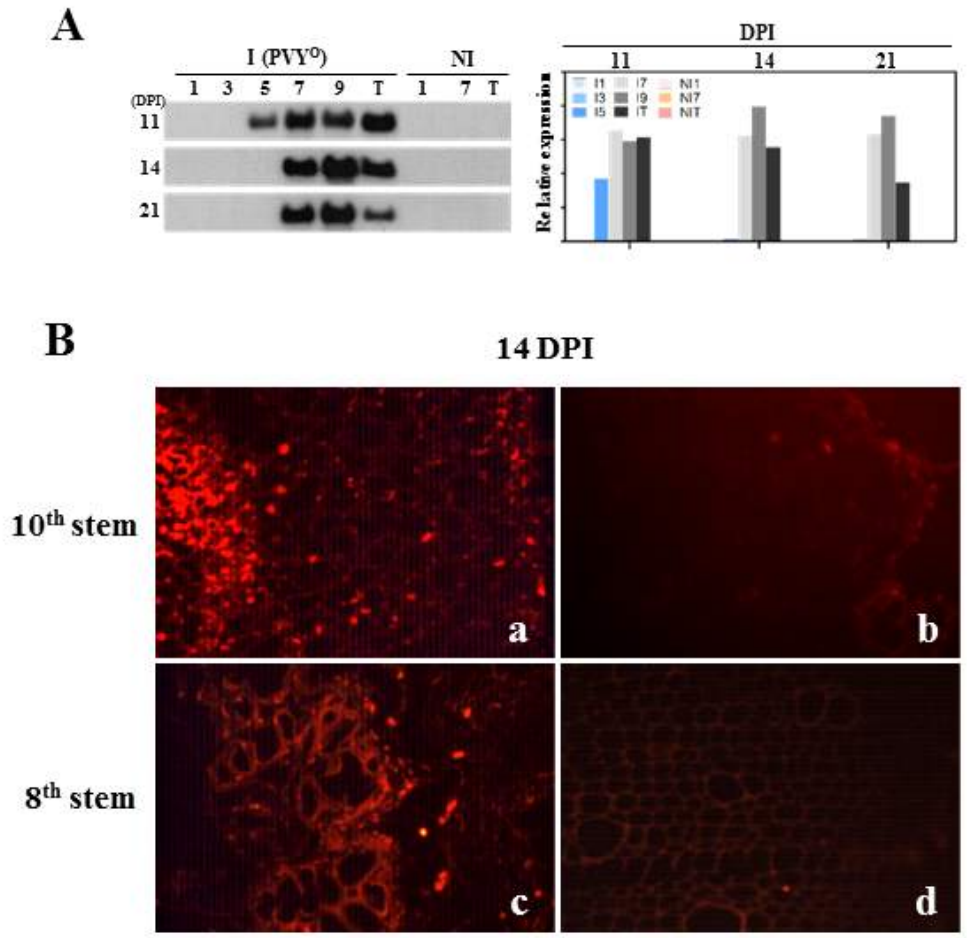

Figure 1.5. PYY coat protein (CP) accumulation in infected *N. benthamiana* plants with PVY^{O}. (A) Western blot analysis of the PVY coat protein (CP) accumulation in infected *N. benthamiana* plants (Left). Lanes are as follows: the systemic leaves of infected plants (I) and un-inoculated healthy plants (NI). Numbers represent the leaf number. Right, Virus contents were measured using Image J. The y axis indicates relative expression level. **(B)** Immunolocalization of viral coat protein in the stems at 14 DPI. **a**, 10th stem in PVY^{O} infected plant at 14 DPI; **b**, control as in **a**; **c**, 8th stem at 14 dpi; **d**, control as in **c**.

1.4.3 Morphological changes observed in top leaves after PVY^O infection

To observe morphological changes of leaves during PVY^O infection, 8^{th} and 10^{th} leaves of 9 and 14 DPI plants were collected. Collected leaves were made into Epon block through primary fixation, secondary fixation, dehydration, infiltration and embedding process. Epon block was cross-sectioned to 1 μm thickness using a microtome. The semi-sections were observed after staining with 1% toluidine blue. (Fig 1.5). As a result of the observation, cross-section fragments could be used to observe the structure of control and infected plant leaves. The plant structure consists of upper epidermal cells (top figure in Fig 1.5.A), palisade parenchyma (middle figure in Fig 1.5.A), and vascular bundle within the spongy parenchyma layer. When the 8^{th} leaf of 9 DPI was compared to healthy normal plant leaf, the number of cells of the spongy parenchyma layer of the infected plant leaf was reduced compared to the number of normal plants. In the case of 8^{th} leaf on 14 DPI, the cells inside the leaf were arranged irregularly and their intercellular space as expanded compare to the 8^{th} leaf on 9 DPI. A more definite change was observed in the 10^{th} leaf of 14 DPI. Compared to the infected plant, the cells uninfected were small and compact, and the arrangement of the cells was irregular due to massive cell division. In addition, decreased number of cells inside the leaf and slow growth of the leaves, were reflected in a difference in leaf thickness at infected plants (Fig 1.5.B).

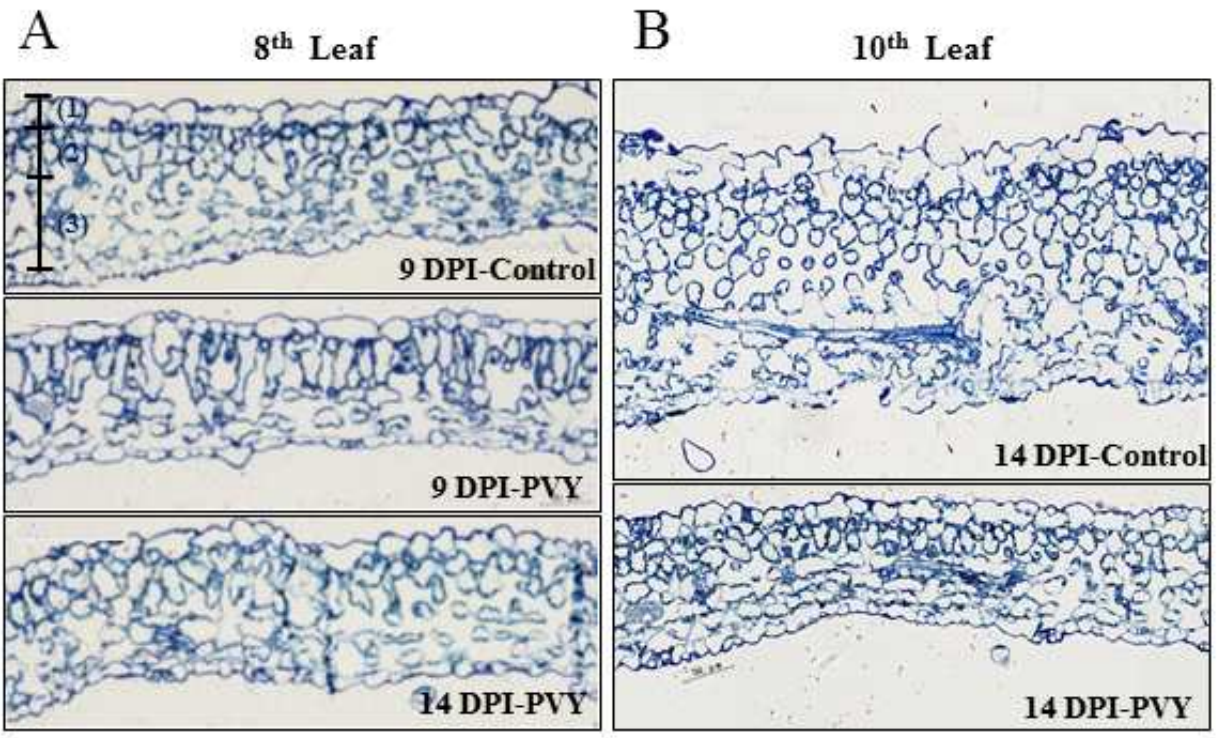

Figure 1.6. Anatomical structure of systemic leaves in *Nicotiana benthamiana* infected with PVY^{O}. (A) Cross section of the eighth leaf above the inoculated leaf. **(B)** Cross section of the 10th leaves under light microscopy. Upper epidermal cells (1), palisade parenchyma (2), and a vascular bundle within the spongy parenchyma layer (3) are indicated. All scale bars represent 100 nm.

1.4.4 Observation and localization of micro-organelle and PVY^{O} in upper leaves using TEM

A thin section for electron microscopy was performed using the epon block used in the semi-thin section. The thin section was conducted in the tissue near the vascular bundle where virus particles mainly appeared (Fig 1.4.B). The sample was cross-sectioned with a diamond knife to a thickness of 100 nm. The sample on the grid was cross-stained with 4% uranyl acetate. Samples were observed at 50 kV using a JEM-2000 FXⅡ electron microscope (JEOL Ltd., Tokyo, Japan) at the Department of Pathology, Chonnam National University Hospital. Observations were observed from 3000 magnifications to 60,000 magnifications. Abnormal structures were identified specifically in cells near the vascular bundle of infected plants (Fig 1.7.C). The enlargement of the abnormal site was observed, and the symptoms of potyvirus infection were observed. Characteristically, pinwheel structure and scroll structure were observed (Figure 1.7.b). The viral constructs occupied a large part of the cytosol, representing that PVY^{O} has been infected. Ultrastructural analysis revealed expanded endoplasmic reticulum (ER) structure that obstructed by adjacent virus particles. It represents that the dilated ER in infected cells is associated with ER stress. These results suggest that ER stress may be induced in virus infected cell and ER stress associated autophagy may take part in the pathophysiology of infected plants. Since the ER is the platform of autophagosome formation, dynamic virus association may have a role in providing components required for removal process of virus particles. Large size of high-density particle that enclosed with multiple-layers of membrane structure was found in the autophagosomes, observed in the 8th leaf at 9 DPI (Fig 1.7.B). The

pinewheel structure was also found in vascular cell next to vascular-fibers, suggesting the movement of the virus particle through phloem cells. Moreover, autophagosome formation was localized at the site of chloroplast. The autophagosome associated chloroplast membrane caused disruption of internal-membrane structure of chloroplasts (Fig 1.7.C) The form of the infected chloroplast was destroyed and had an abnormal internal structure. Autophagosome formation was highly observed in infected cells (Fig 1.7.c'). Autophagosomes were observed in cells where some infections were seen (Fig 1.7. top fig). In the case of non-infected normal cells, the shape of the organelles was constant, and transparent autophagosome was observed in the cells (Fig 1.8).

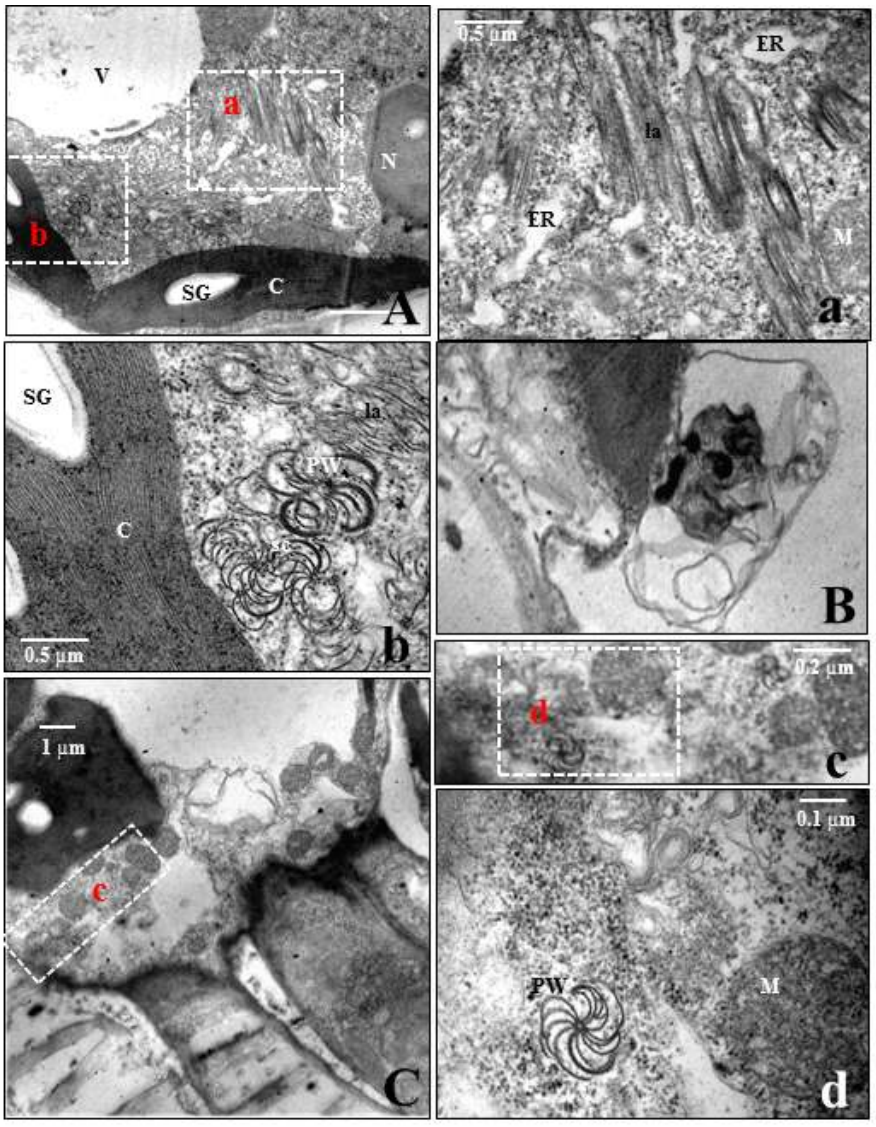

Figure 1.7. Transmission electron micrographs of cytoplasmic inclusions in the cytoplasm of PVY^{O} -infected tobacco. Tobacco (*N. benthamiana*) were mechanically inoculated with the PVY^{O} and the 8th leaf above the inoculated leaf prepared for electron microscopy at 9 DPI. **(A)** Pinwheel (pw), scroll (sc) and laminated aggregate (a) cytoplasmic inclusions are clearly visible in the cytoplasm of PVY-infected tobacco leaves. (B) Autophagosome (C) Pinwheel in phloem. Vacule (V), starch grain (SG), chloroplast (C), endoplasmic reticulum (ER), mitochondria (M). Scale bars represent as indicated.

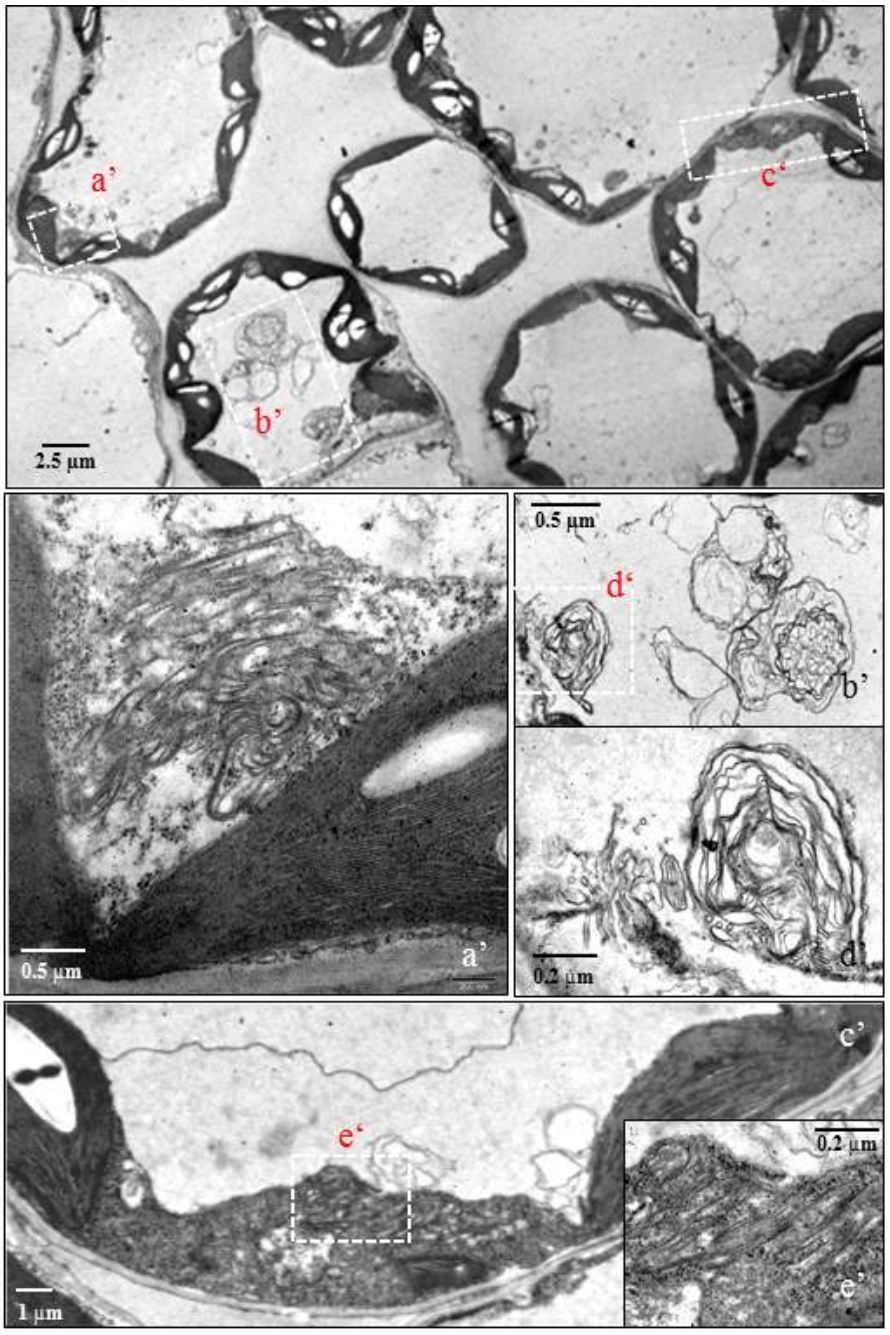

Figure 1.8. Transmission electron micrographs of cytoplasmic inclusions in chloroplasts of PVY^{O} infected tobacco. The 10th leaf above the inoculated leaf prepared for electron microscopy at 9 DPI. Scale bars represent as indicated.

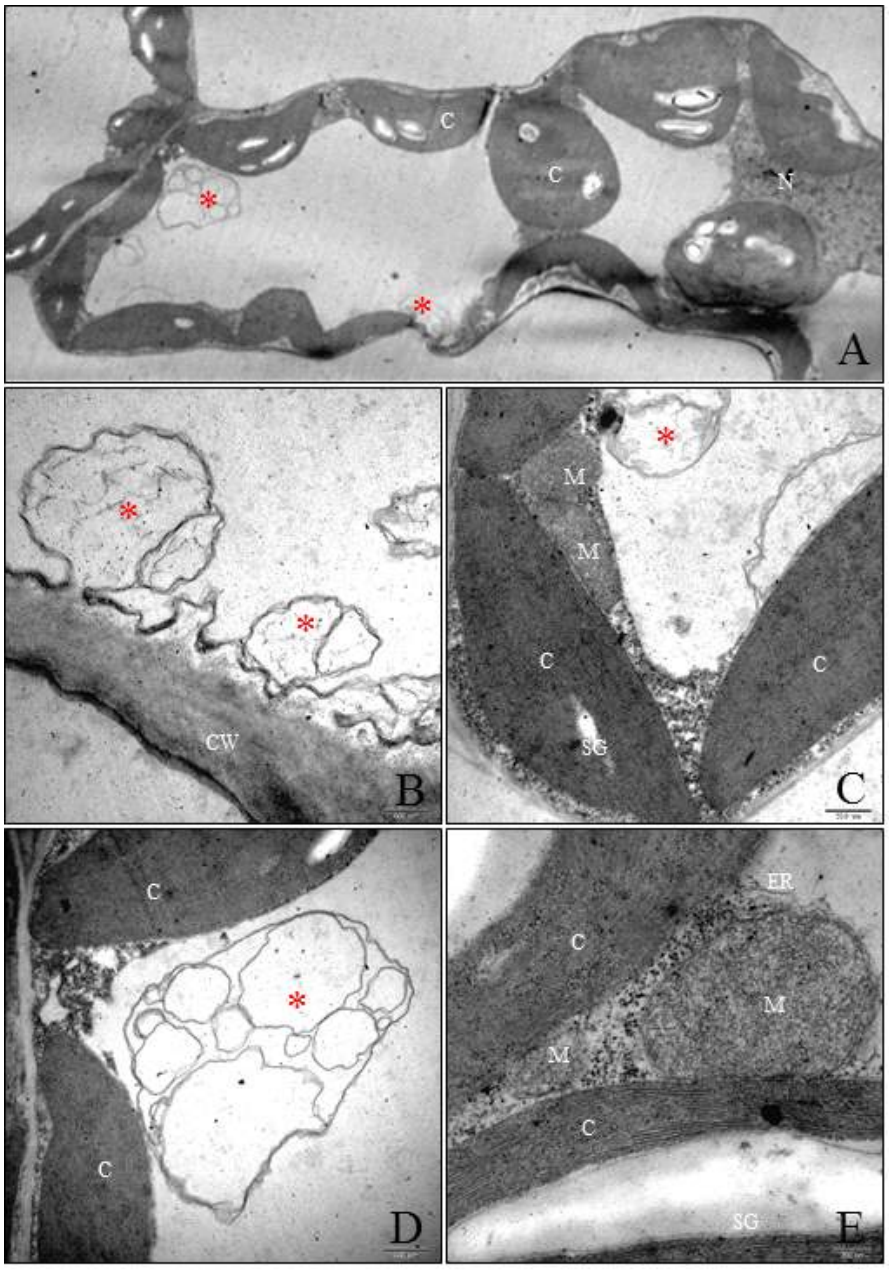

Figure 1.9. Transmission electron micrographs of autophagosomes in healthy leaves of *N. benthamiana*. The 8th leaf was observed from healthy tobacco plants. The areas delineated by white rectangles in the top panels are shown at higher magnification in the bottom panels. Red stars represent the autophagosome. Scale bars represent as indicated.

1.4.5 ROS production in tobacco plants after viral infection

When infected with a pathogen, the organism will produce ROS. In the study, I investigated whether the infection of tobacco plants with PVY^{O} lead to massive gerneration of superoxide, which is proceeded by the production of hydrogen peroxide, resulting the activation of defense mechanisms. For this, after PVY^{O}, infection leaves at 1, 5, and 7 DPI were stained with nitro blue tetrazolium (NBT). The result showed that virus inoculation caused severe superoxide generation in the whole leaves. As shown in Fig 1.9, histochemical detection of superoxide showed that cell spots were stained intense blue after virus infection. In contrast, NBT precipitation was not visible in the leaf blade of uninfected plants. Generation of superoxide increased dramatically in the plant at 1 day after virus infection. It was confirmed that ROS was generated mainly in vein. The amount of ROS was decreased in the lower leaves as time passed after PVY^{O} infection. However, in the upper leaves, the amount of ROS was decreased, but ROS still appeared. Additionally, in the upper leaf of 5 DPI, there was small unstained space in the center of NBT-stained area, representing the formation of mocri-lesion in the systemic leaves.

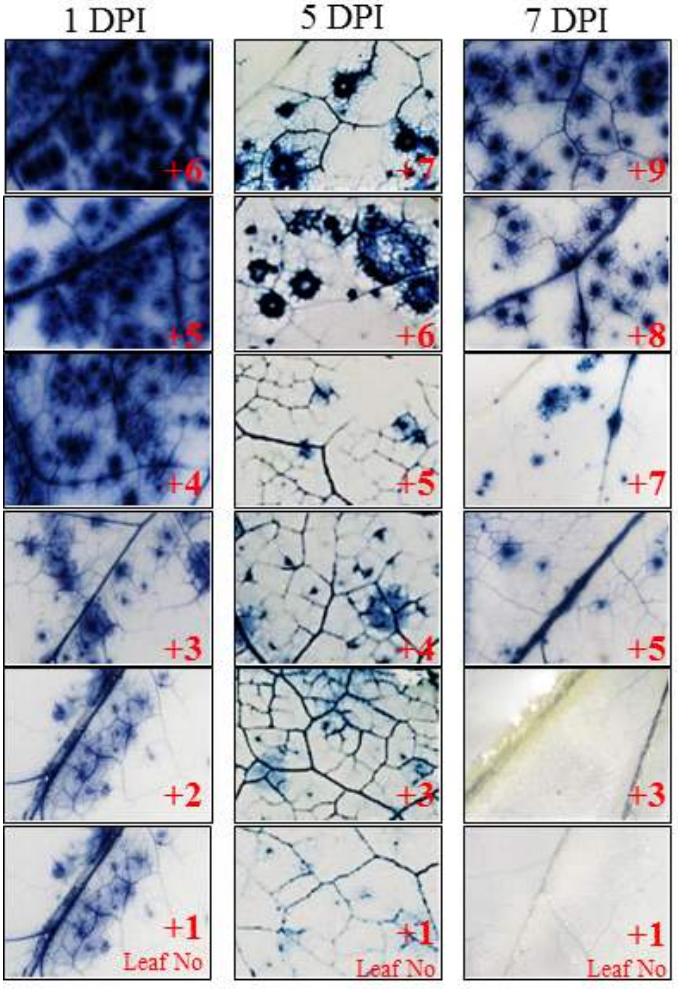

Figure 1.10. Detection of superoxide accumulation in infected leaves of *N. benthamiana* with PVY^{O}. The numbers are represent the order of systemic leaves above the infected leaf at indicated days (1, 5, 7 DPI).

1.4.6 Induction of antioxidant enzymes in the leaves of tobacco after virus infection

Under viral infection, the actual level of reactive oxygens was incresed dramatically compared with healthy plants, especially within the sites of localization of antioxidant enzymes. SOD isoenzymes and H_2O_2-scavenging enzymes were preferentially located near the site of ROS production. Massive generation of superoxide was observed in all the leaves as the plants were infected with PVY^O. Then, the amount of superoxide decreased over time, especially in the lower part of the infected plants. Therefore, the expression level of ROS scavenging-related proteins was examined in the systemic leaves of tobacco plants 3 hours after PVY^O infection. A simultaneous analysis of the response of each SOD isoenzyme was conducted. Among the SOD isoenzymes, two chloroplast SOD (CSD2 and FeSOD), and a mitochondrial SOD (MnSOD) were tested. The antibody information used in this experiment is shown in Table 1.3. The steady-state protein level of chloroplast SODs markedly increased in the systemic leaves of infected plants in response to viral infection, but not in uninfected control plants. The MnSOD levels did not changed in response to the viral infection. The results indicate that superoxide generation occurred mainly in the chloroplast. However, the expression of ChlAPX and cAPX, as well as cytosolic catalase (CAT) was highly enhanced for efficient detoxification of H_2O_2 under the biotic stress condition.

These results support that the expression of CSD2, FeSOD, APX, and CAT was up-regulated in response to cellular ROS levels. The accumulation of ROS may play an important role in the regulation of antioxidant gene expression under the

biotic stress condition. Upon virus attack, ROS including superoxide and H2O2 can help to induce cell death in the infected cells or serve as a signal to activate defence responses in distant uninfected tissues. In addition, Lhca1 and Lhca2 showed similar expression level in the systemic leaves (Fig 1.10.A).

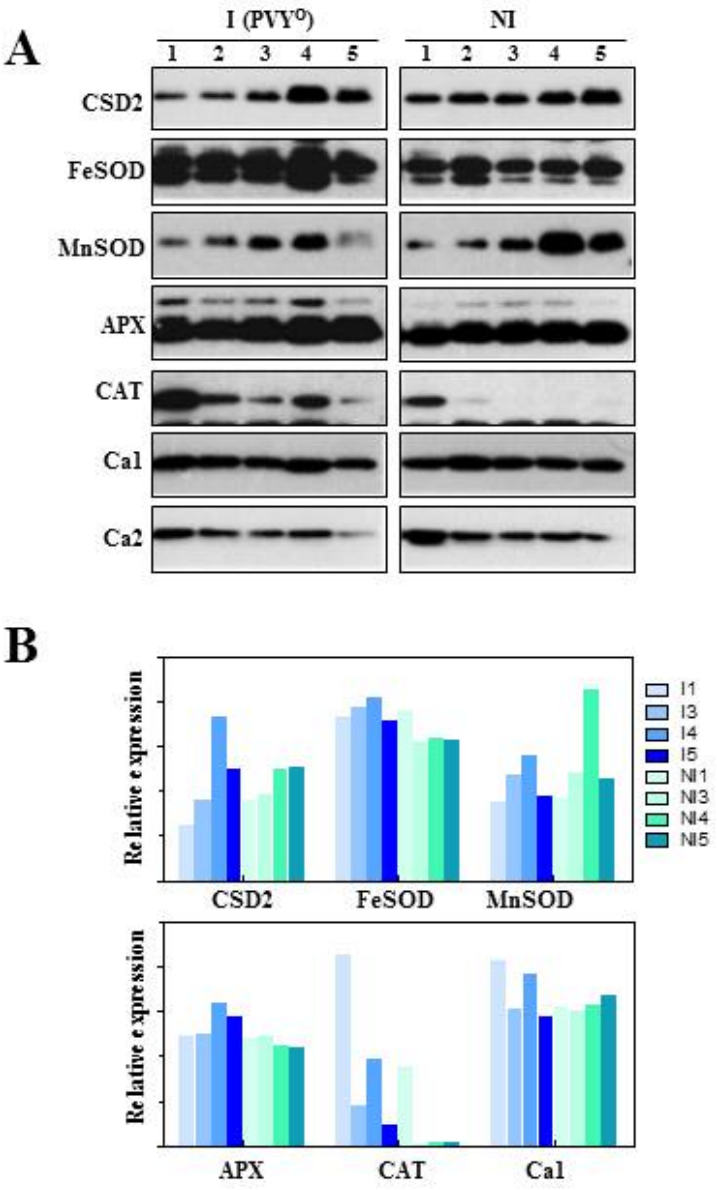

Figure 1.11. Effect of PVY^{O} on antioxidant enzymes in systemic leaves of *N. benthamiana* infected with PVY^{O}. The numbers represent the order of systemic leaves above the infected leaf at 3 hours post-inoculation (HPI). **A**, Expression levels of antioxidant enzymes. Protein extracts were prepared from the leaves for Western blot analysis to determine the levels of protein accumulation. **B**, Quantitative results of '**A**'. **I**, infected leaves with PVY^{O}; **NI**, non-infected healthy leaves as control.

1.4.7 Change in hydrogen peroxide scavenging enzyme levels in response to virus infection

To establish systemic analysis of ROS scavenging enymes in response to viral infection, I performed immunoblot analysis , representing ascorbate peroxidase (APX) and catalase (CAT) expression in infected tobacco plants. Total protein was prepared for immnoblot analysis from control and virus-infected plants on 7, 9, 11, 14, and 21 DPI. The experiments have focused on the changes in the level of APX and CAT in the each leaf of tobacco tobacco from the base to apex at different time course. APX and CAT analyzed following virus infection, their expression levels were found to be significantly increased until 9 DPI, whereas overall expression levels were decreased from 11 DPI. Interestingly, APX levels were significantly increased along the leaf position to the apex of infected plants in response to the biotic stress . However, enhanced expression of CAT was observed in the systemic leaves on 11 DPI, which may induced along with mosaic symptom development in the young leaf on apex of the plant (Fig 1.11). However, the expression level decreased at 14 DPI when the symptoms appeared. In general, expression of APX and CAT decreased with time in the lower leaves.

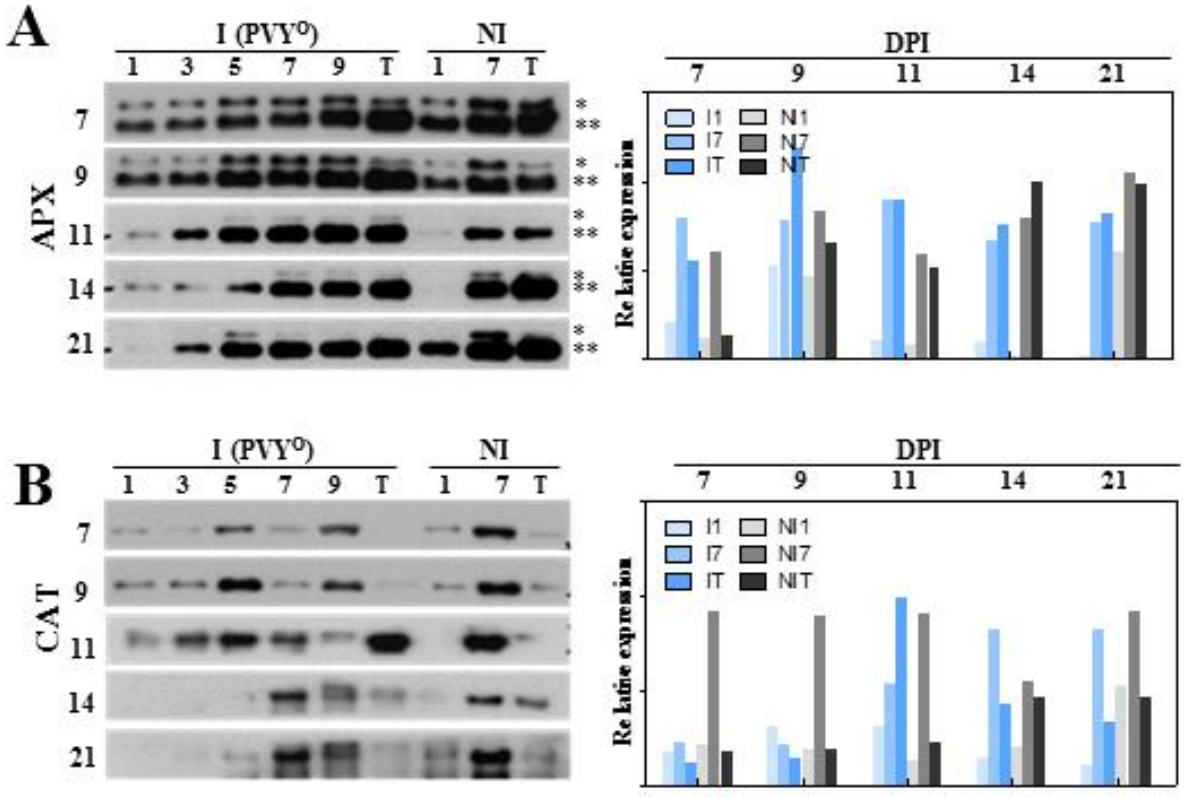

Figure 1.12. Effect of PVY^{O} on antioxidant enzymes in systemic leaves of *N. benthamiana* infected with PVY^{O}. The numbers represent the order of systemic leaves above the infected leaf at indicated time. **A**, Ascorbate peroxidase (APX). **B**, Catalase (CAT). Protein extracts were prepared from the leaves for Western blot analysis to determine the levels of protein accumulation. Right panel, quantitative results of western blot. **I**, infected leaves with PVY^{O}; **NI**, non-infected healthy leaves as control. Asterisk of left panel means to peroxisomal (*) and cytoplasmic (**) APX

1.4.8 Expression of autophagy-related proteins in virus infected plants

In this study, the expression level of the proteins involved in the formation of autophagosome was examined in tobacco plants after the virus infection. In the autophagy pathway, a double-membrane vesicle called autophagosome encloses intracellular cargoes to deliver them into the vacuole. ATG proteins are involved in a series of autophagy events and often function as complexes. For instance, cysteine protease ATG4 cuts ATG8 to produce cytosolic ATG8. The truncated ATG8 is combined with phosphatidylethanolamine (PE) to form lipidated ATG8. In this experiment, the induction of ATG4 was detected in the upper part of the infected plants, which is same location of virus protein accumulation. However, the expression levels of ATG4 and ATG8 were changed with time. When viral symptomes were appeared in the youngest leaf, the expression of ATG4 decreased, suggesting supression of autophagy pathway by disease development (Fig 1.12.B). In the case of ATG8, constitutive expression was observed in the leaves of tobacco regardless viral infection. However, lipidated ATG8 was evidently accumulated from the young leaves and the level was decreased after disease development on 14 DPI. (Fig 1.12.C).

In addition, binding immunoglobulin protein (BIP), an ER stress maker, binds to misfolded proteins to remove abnormal proteins. The protein degradation is critical for modulating numerous biological processes under the stress conditions. When a virus is infected, intense band of BiP was detected in the systemic leaves from upper part of plants. But, over time, the amount of expression decreased slightly, especially in teh lower part of the plants (Fig 1.12.A).

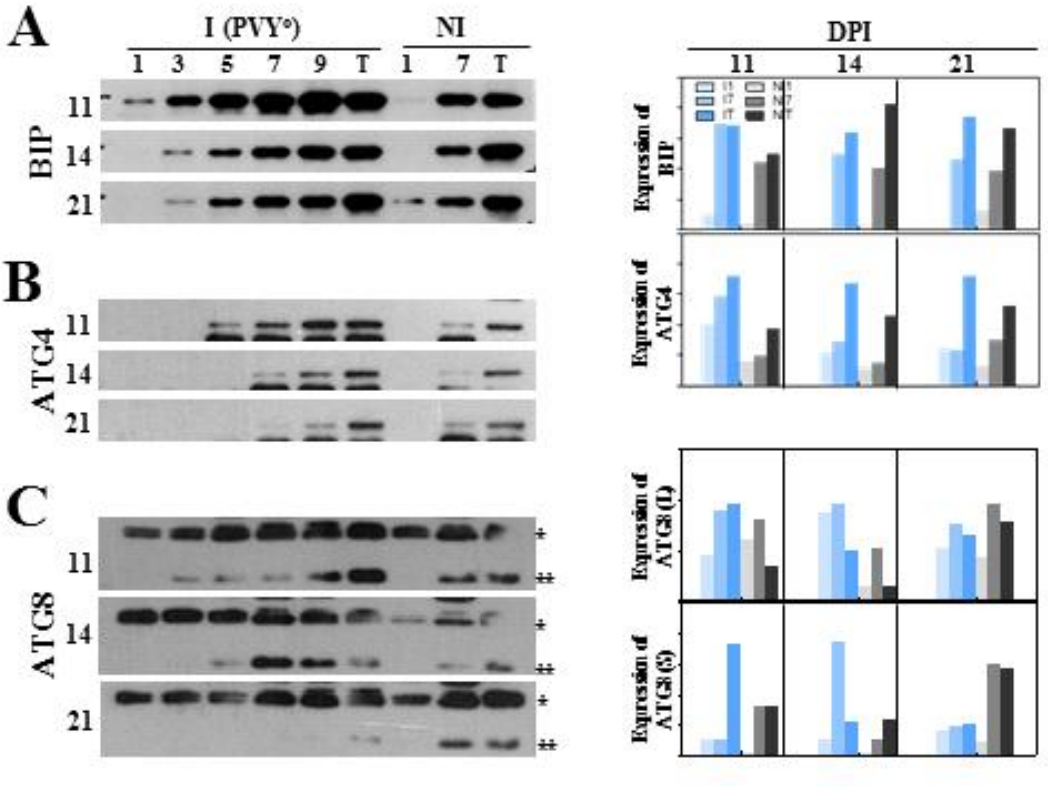

Figure 1.13. Effect of PVY on Autophagy-related proteins in systemic leaves of *N. benthamiana* infected with PVY^{O}. The numbers represent the order of systemic leaves above the infected leaf at indicated time (dpi). **A**, BIP. **B**, ATG4. **C**, ATG8. Protein extracts were prepared from the leaves for Western blot analysis to determine the levels of protein accumulation. Quantitative results of Right panel. **I**, infected leaves with PVY^{O}; **NI**, non-infected healthy leaves as control.

1.4.9 Localization of autophagy-related protein 4 through cross-section of stem after virus infection

Expression of autophagy related proteins was highly induced in the infected tobacco plants after PVY^{O} infection. (Fig 1.12.B and C). Immunolocalization was performed on transverse sections of the stem from both infected and uninfected plants in order to localize ATG4 protein. Paraffin sections were prepared from the 10th leaf stem of infected plants and normal plants harvested at 9 DPI. Anti-ATG4 was attached to the section and goat anti-rabbit IgG conjugated rhodamine red X was used to observe under a fluorescence microscope. Under normal conditions, ATG4 accumulation was rarely detected in the stem cells of both plants. Thus the deposition of ATG4 was examined in the vascular bundles that was known as virus path. Following virus infection, massive accumulation of ATG4 was observed in the cells around vascular tissues of the infected plants. The result suggests that ATG4 proteins were colocalized with PVY^{O} and may involved in the autophgosome formation in the presence of virus particles. No immuno staining was observed in control sections incubated with pre-immune serum (data not shown).

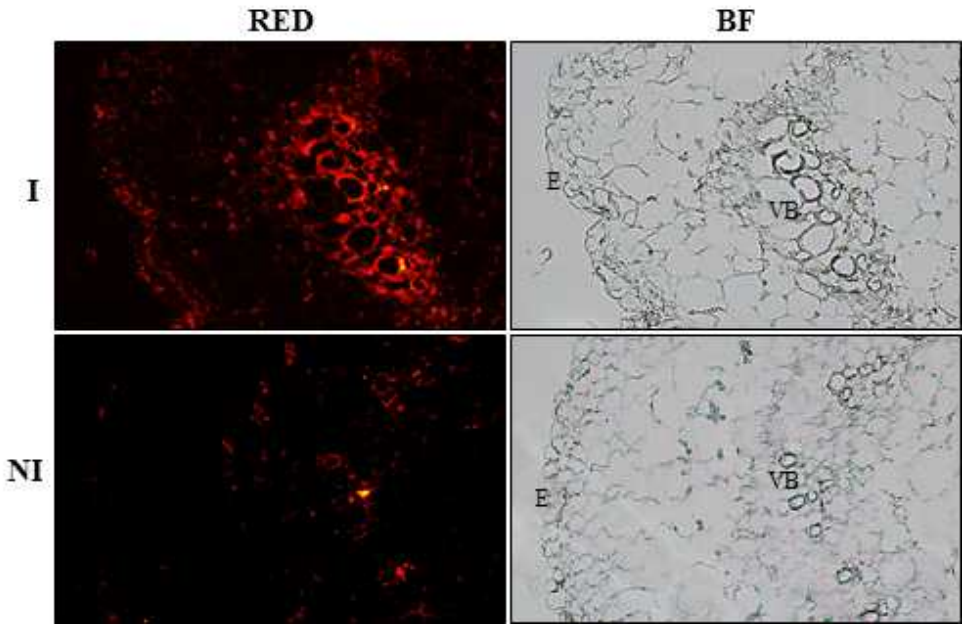

Figure 1.14. Immunolocalization of ATG4 in the stem of *N. benthamiana* infected with PVY^{O}. RED, red fluorescence. BF, bright field. I, infected leaves with PVY^{O}. NI, non-infected healthy leaves as control. Epidermis cells (E), Vascular bundles (VB).

1.4.10 Expression pattern of RNA suppression-related genes

RNA silencing is an ubiquitous defense mechanism that is activated by non-coding RNAs or double-stranded RNAs (dsRNAs). dsRNA-mediated sequence-specific mRNA degradation has been recieved attention in antiviral defense. Majority of plant viruses possess a single-stranded RNA genome that is amplified through dsRNA intermediates. In response to viral invasion, plants can recognize the dsRNA of the virus and have evolved RNA silencing pathway as a defense mechanism against the viruses. Viral dsRNAs are cleaved by dicer-like (DCL) enzymes into small interfering RNAs (siRNAs) that guide to the target viral RNA. The target RNA is then degrade by argonaute (AGO) proteins. Thus siRNAs are likely to be the mobile signal that spreads the defense response to prevent viral accumulation in systemic leaves.

Expression levels of genes involved in viral RNA suppression in infected plants were determined. RNA was extracted from 3, 7 and 9 leaves of infected plant on 11 and 14 DPI. RNA was converted to cDNA and expression levels of AGO1, AGO2, DCL2, DCL4 and ATG4 were determined. The result showed that the expression level of AGO1 decreased from the 9th leaf of 14 DPI plant than in 11 DPI plant. AGO2 showed a very weak expression level as a whole. Similar to AGO1, expression of DCL2 was decreased in 9th leaves of 14 DPI plants than in 11 DPI plants. The expression level of DCL4 was weak except for the 3rd of 11 DPI. In the case of ATG4, 14 DPI showed weak overall expression.

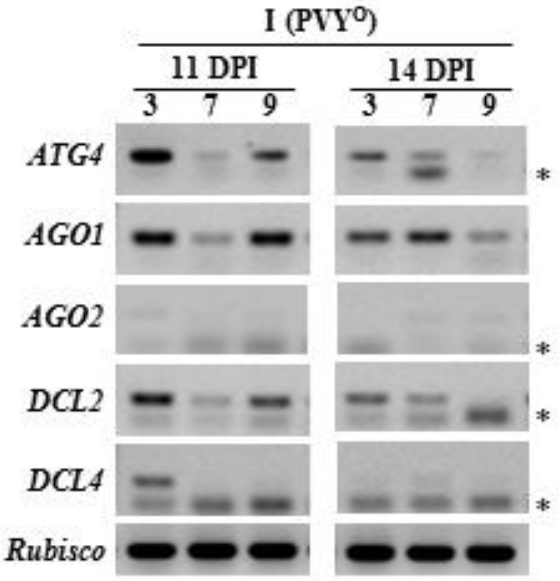

Figure 1.15. RT-PCR analysis of viral defense related genes in the leaves of *N. benthamiana* infected with PVY^{O}. RNA extracted in 11 and 14 DPI plants leaf. The leaf number is indicated above the inoculated leaf (3, 7 and 9). Autophagy relative gene 4 and 8 ATG4, 8; Argonaute 1 and 2, AGO1, 2; DCL 2 and 4, dicer-like protein 2, 4; Rubisco, Ribulose-1,5-bisphosphate carboxylase/oxygenase. **I**, infected leaves with PVY^{O}; Rubisco was used as loading control. Primer dimers marked by an asterisk (*).

1.4.11 Expression levels of pathogen related protein 3 and chlorophyll binding protein in infected plants

Plants respond to invasions of phytopathogens with coordinated gene expression. Various genes are induced both at the site of infection and in distal parts of the plant, leading to development of the hypersensitive reaction (HR) and systemic acquired resistance (SAR), respectively (Jackson and Taylor 1996, Durrant and Dong 2004). The expression levels of several genes are often used as indices of plant resistance to pathogen infection. For example, pathogenesis-related (PR) genes are induced early, at higher levels, during incompatible host-pathogen interactions than during compatible interactions (Bell, 1986). PR proteins do not usually accumulate in healthy plants, but are induced by pathogen infection or related stresses, and improve the defensive capacity of plants (Loon and Strien, 1999).

The expression level of pathogenesis related protein 3 (PR3) was determined in infected plants on 11, 14 and 21 DPI. At 14 DPI, the expression of PR3 protein was detected in the leaves of infected plants, except the youngest leaf, suggesting suppression of PR3 expression. The expression level was significantly increased at top leaves of 14 DPI than 11 DPI. However, it was shown that the expression level decreased again after 21 DPI. In addition, on 11, 14 and 21 DPI, the infected plants were examined to clarify chlorophyll binding protein changes due to the effects of the virus. In the case of LhCb, there was no significant change over time after infection.

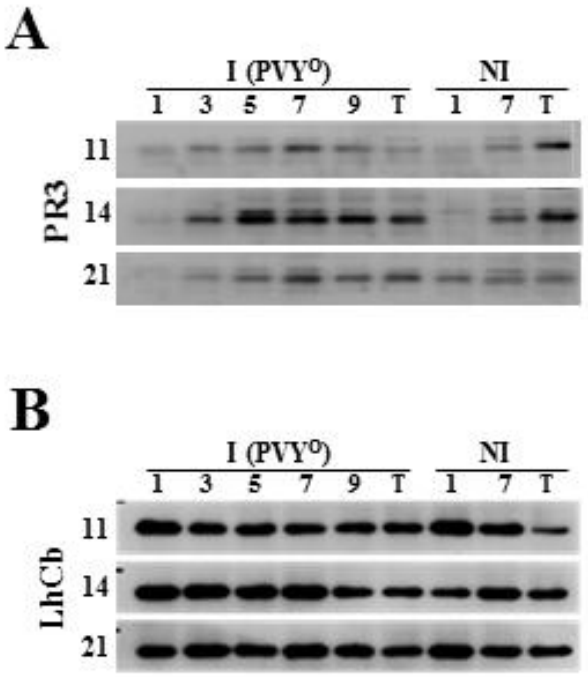

Figure 1.16. Effect of PVY^{O} on pathogenesis related protein 3 (PR3) in systemic leaves of *N. benthamiana* infected with PVY^{O}. The numbers are represent the order of systemic leaves above the infected leaf at indicated time (DPI). **A**, Expression levels of PR3 protein. Protein extracts were prepared from the leaves for western blot analysis. **B**, Expression levels of chlorophyll binding protein, LhCb. **I**, infected leaves with PVY^{O}; **NI**, non-infected healthy leaves as control.

1.4.12 Constructions for transgenic *N. benthamiana* including autophagy-related genes

In order to study the interaction between autophagy and virus in virus infection, I tried to make transgenic mutant. To isolate target genes, *ATG5* and *ATG8f* genes of *Nicotiana benthamiana* were identified by homology search. The *ATG5* and *ATG8f* genes of *Arabidopsis thaliana* were investigated in The Arabidopsis Information Resource (TAIR, https://www.arabidopsis.org). Based on the *ATG5* and *ATG8f* sequences of *A. thaliana*, sequences of *Nicotiana tabacum* and *Nicotiana benthamiana* were investigated in the National Center for Biotechnology Information (NCBI, https://www.ncbi.nlm.nih. gov). Each sequence was used for a homology alignment after translation. Homology research was performed using the Clustal Omega tool from The European Bioinformatics Institute (EMBL-EBI, https://www.ebi.ac.uk). In ATG5, the homologies of *A. thaliana*, *N. tabacum* and *N. benthamiana* were 63.8% and 64.39%, respectively. The homology between *N. tabacum* and *N. benthamiana* was 95.15% (Fig 1.16). In ATG8f, the homology of *A. thaliana*, *N. tabacum* and *N. benthamiana* was 89.26% and 92.52%, respectively. Homology of *N. tabacum* and *N. benthamiana* was 96.3% (Fig 1.17)

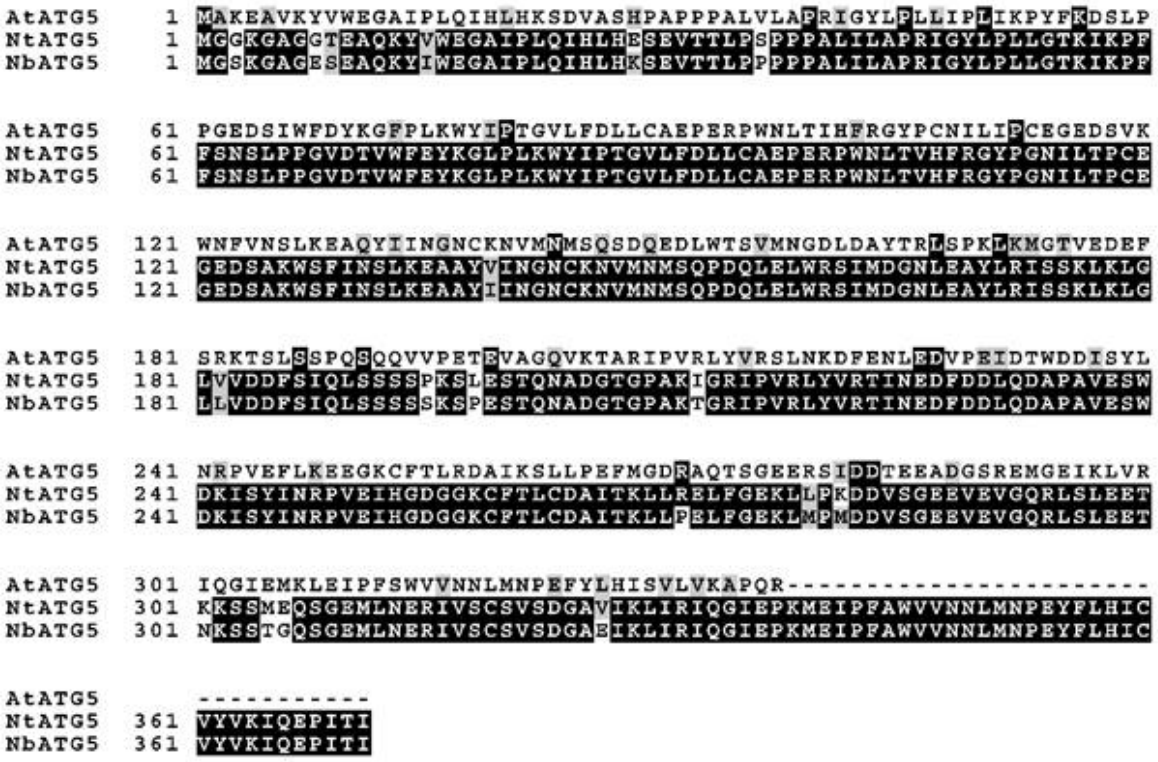

Figure 1.17. Alignment of amino acid sequences of autophagy-related gene 5 proteins from different species. AtATG5 (*Arabidopsis thaliana*, accession no. NM_121735.5), NtATG5 (*Nicotiana tabacum*, accession no. KR336562), NbATG5 (*Nicotiana benthamiana*, accession no. KX369397.1)

Figure 1.18. Alignment of amino acid sequences of autophagy-related gene 8 proteins from different species. AtATG8f (*Arabidopsis thaliana*, accession no. NM_117751), NtATG5 (*Nicotiana tabacum*, accession no. JX175260.1), NbATG5 (*Nicotiana benthamiana*, accession no. Niben101Scf03374g01007.1)

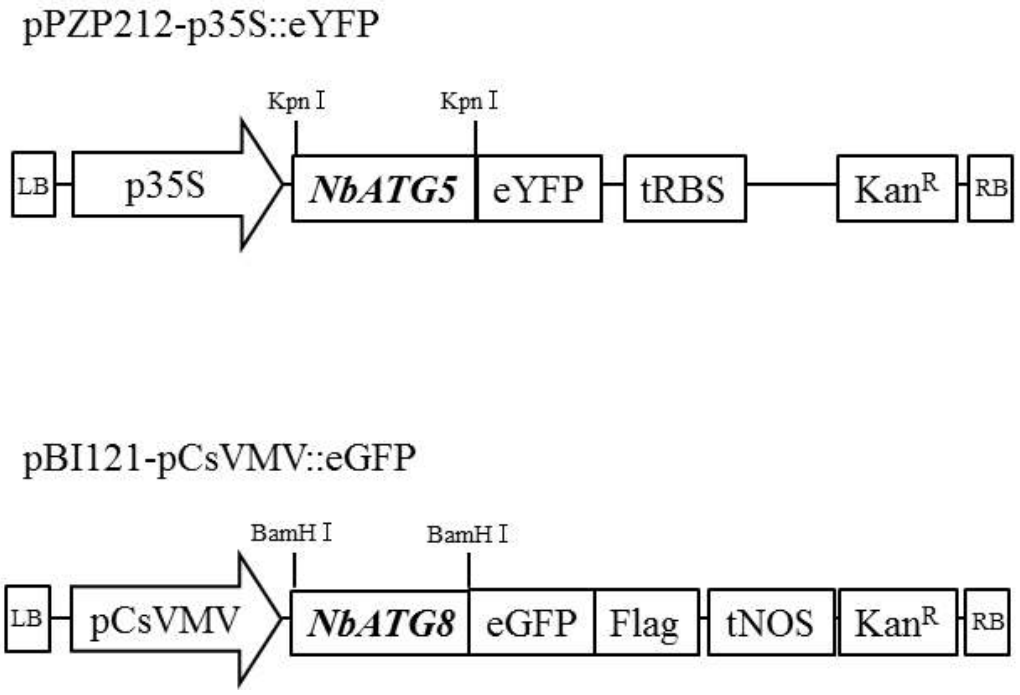

Figure 1.19. Constructions of autophagy-related genes of *N. benthamiana* in binary expression vector. *N. benthamiana ATG5* and *ATG8* genes cloned into binary expression vectors. Vectors were composed of LB and RB borders, promoter, reporter genes, terminator, bacterial and plant selection markers. Promoter derived from plants mosaic viruses (*Cauliflower mosaic virus*-35S and *Cassava mosaic virus*-CsVMV promoters). Kanamycin resistance gene was used as transformed plants selection marker. Kanamycin and spectinomycin were used as transformed bacterial selection markers.

1.5 DISCUSSION

After PVY^{O} infection, I followed the reactions occurring in the plant by leaf position and time. *N. benthamiana* infected with PVY changed its molecular pattern on the 14^{th} day. The plants infected with the virus exhibited the growth retardation of newly growing leaves (Fig 1.1, 1.2 and 1.3). Because maybe the virus delays translation of the host for its replication (Christophe, 2006). When the leaves were cross-sectioned using a semi-thin section, the number of mesophyll cells was significantly less in the infected leaf than in the control leaf (Fig. 1.6). These results may be due to inhibition of cell growth, but may also be due to viruses.

ELISA data shows the movement of the virus (Fig. 1.4). PVY viruses proliferate over time in the top leaves. The proliferating virus slowly comes down to the lower leaves. The transfer of the virus to neighboring cells uses plasmodesmata (Lee, 2011, Amit, 2015). From the PVY coat protein western blot results and the IHC results of the 14 DPI stem, it is clear that the virus is detected in the upper part of the plant and virus is used vascular bundle system (Fig 1.5). Experimental results suggest that the virus is directed to the top leaf of the plant by not only phloem but also certain elements (ex; auxin gradient, growth factor). It seemed to be closely related to the growth of the plant, especially the viral particles in the newly growing leaves.

The location of the virus and the morphology of cell organelles were observed in the TEM experiments (Fig 1.7, 1.8 and 1.9). Potiviruses are known to be distributed in plant cell organelles such as cytosol, ER, vacule, and chloroplast (D

Riedel, 1998, M Sorel, 2014, Frederic, 2015). TEM images showed that PVY^O was localized in cytosol, ER, chloroplast and vascular bundle. (Fig 1.7). And these images showed pinwheel, scroll and laminated aggregation, which is a specific structure in potyvirus infection (Fig 1.7 and 1.8). When infected with PVY^O, more starch grains accumulated in chloroplast than control. Infections of plant viruses inhibit the migration of starch in chloroplasts (Liu, 2016). The accumulation of starch grain by viruses is not yet known. However, starch grain is a major energy source of the plant and is transported to all parts of the plant. In this respect, it is thought that there is a relation with the movement of virus.

ROS plays an essential role in cell defense mechanisms. High concentrations of ROS act as signals that cause apoptosis (María, 2012). Rapid increase in ROS occurred at the early time (1 DPI) after virus infection. The ROS level remained high in the 5, 7 DPI, but the ROS level in the lower leaves decreased. However, the ROS level remained high in the upper leaves (Fig 1.10). The expression level of the enzymes to remove intracellular ROS was higher than that of control, especially in chloroplast. (Fig 1.11). Perhaps it is thought to remove ROS immediately to reduce intracellular damage, but it is thought to be exposed to continuous damage by virus. Even after 7 DPI, the level of APX acting on ROS scavenging was still high. Catalase was weakly expressed than APX. However, the strongest response was seen in the top leaf of 11 DPI before infection. High expression levels in the upper leaves may also be associated with movement of the virus.

ER stress activates the action of autophagy in plant and mammalian cell. ROS is a major cause of ER stress, and another cause is the accumulation of mis(un)folded protein in the ER. (Lee, 2012, Rashid, 2015, Ozgur, 2018). BiP is a

protein in the ER that reacts with unfolded protein and is responsible for the degradation of abnormal proteins. BiP is not only involved in the movement of viruses, but it is also involved in virus infection (Ye, 2011, Yan, 2017). BiP is associated with infection of the virus and the activation of autophagy. The expression level of BiP increased from 11 DPI to infection decreased over time (Fig 1.13.A). It is also associated with the autophagosome forming factor ATG8. At 11 DPI, ATG8 is cleaved by ATG4 to produce a large amount of ATG8-PE form. However, ATG8-PE formation was significantly reduced in the late stage of infection (Fig 1.13.C). ATG4, a Cys protease, also decreased in expression over time (Fig 1.13.B). What this means is that as infections become more severe, the function of autophagy decrease more. The BiP function also has the same features as a double-edged sword. While there is a mechanism that acts to break down the protein of the virus, not the protein of the host, and it is also involved in the migration of the virus protein. As a result, it is suggested that the defense mechanism of the plant is inhibited by virus over time after virus infection.

Virus movement is cell-to-cell or long-distance movement as mentioned above. The expression of ATG4 through leaf cross-sections was determined. ATG4 was specifically over-expressed in the periphery of the vascular bundle (Fig 1.14). The long-distance movement of the virus indicates that it is closely related to autophagy.

Host defense mechanisms against plant virus mainly are viral RNA silencing. Viral RNA silencing is carried out by host DCL (dicer like) proteins and AGO (argonautes) proteins. DCL recognizes viral dsRNA and then cleaves and produces 21-23 short nucleotides. The nucleotides bind to viral ssRNA by AGO. AGOs form RISC (RNA-induced silencing complex) whereby viral RNA is either

transcriptionally inhibited or degraded (Pallas, 2011, Ghoshal, 2015, Valli, 2018). The expression levels of *DCL2*, *DCL4*, *AGO1* and *AGO2* genes were investigated by gene specific primers in *N. benthamiana* infected with PVY^{O}. DCL2 and DCL4 showed a high level of expression at 11 DPI before the onset of symptoms, but the expression level decreased at 14 DPI, where infection symptoms began to appear. In particular, it showed a dramatic decrease in the top leaves of the plant (Fig 1.15). AGO1 showed strong expression at 11 DPI as well as DCL, but weak expression at 14 DPI. The appearance was remarkable in the upper leaf of the plant. In the case of AGO2, the expression level was very low. ATG4 expression level also decreased after the symptoms appeared. These phenomena indicate inhibition of autophagy. All of these processes were most prominent on the virus-rich upper leaves.

Plant photosynthesis is unique to green plants and is the process of producing nutrients in chloroplasts. The Photosystem is divided into PS I and PS II, and is embedded in the thylakoid membrane inside the chloroplast (Rhee, 1998, Ben-Shem, 2003). PS I and PS II have a light harvest complex (LHC) that collects light. LHC is an essential component for the electron generation required for photosynthesis (Ruban, 2003). Virus-infected plants have been reported to be affected by viruses in the photosystem (Rahouteia, 2000). Early stage in viral infection, LHCa2 reduction was observed in 3 hpi plants, but LHCa1 did not decrease (Fig 1.11). At 11, 14, and 21 DPI, LHCb protein levels were not decreased according to PVY^{O} infection (Fig 1.16.B). In previous reports, plant infections caused by plant viruses were reported to affect only PS II, but there were no reports related to PS I. These results are in contradiction with previous reports.

The PR gene encodes a variety of anti-fungal proteins including chitinases and glucanases. The PR protein is also expressed when infected with the virus, but it is not known how it responds to the virus (Bol, 1990, Brederode, 1991, Moosa, 2017). In fig 1.16.A, PR3, the chitinase, was the most expressed at 14 DPI in which the symptoms appeared. Expression levels were low at 11 DPI prior to the onset of symptoms and at 21 DPI afterwards. However, strong expression was observed in the top leaf of 21 DPI. These results suggest that there is a relationship between symptom expression and PR protein in infected plant.

This study suggests that plants infected with PVY^{O} are retarded in growth. Especially in the upper leaves, ROS removal, activation of autophagy, and viral RNA silencing are actively occurring before 14 DPI in which the symptoms appear. However, after 14 DPI with symptoms, the defensive mechanism of infected plants decreased. In PR3, the highest expression level was observed at 14 DPI. PVY^{O} is thought to migrate through the phloem, and for whatever reason many virus particles were detected in the upper leaves of the plant. In the initial reaction, plants expressed many anti-oxidant enzymes in order to remove the virus-induced ROS, some of the photosystem were obstructed, and accumulation of starch grain was achieved. Autophagy was also rapidly activated early in the virus infection, but it decreased over time. After the symptoms appear, the ability to defend the plant is greatly reduced. This is presumably due to suppression by the helper component proteinase (HC-Pro) and the viral protein genome-liked (VPg) among the components of the virus.

1.6 REFERENCES

1. NA Kassim, ZAA Nerway, KH Yousif. 2014. Identification of Potato virus Y (PVY) and its economic importance on potato crop., *J. Univ. Zakho*., 2(A):304-309.
2. C Kerlan. Potato virus Y. 2006. *CMI/AAB Descriptions of plant viruses* 414.
3. SPF Ximba, JD Ibaba, A Gubba. 2017. Potato virus Y strains infecting potatoes in the Msinga district in the province of KwaZulu-Natal, South Africa. *Crop Protection*., 96(2017):188-194.
4. AC Fulladolsa, KE LaPlant, LG Russell, OC Amy. 2018. Potato Plants Grown from Minitubers are Delayed in Maturity and Lower in Yield, but are not at a Higher Risk of Potato virus Y Infection than Plants Grown from Conventional Seed. *Am. J. Potato Res*., 95(1): 45-53.
5. EB Radcliffe, DW Ragsdale. 2002. Aphid-transmitted potato viruses: the importance of understanding vector biology. *Am. J. Potato Res*. 79: 353–386.
6. VK Alexander, MG Stewart. 2013. Continuous and Emerging Challenges of Potato virus Y in Potato. *Ann. Rev. Phy*., 51: 571-586
7. BGS Karen, A Scott, C Henryk, P Peter, J Emmanuel, H Thomas, H Barbara, S Keith, C Thierry, A Paul, H Cynthia, DF Gary. 2011. Top 10 plant viruses in molecular plant pathology. *Mol. Plant. Path*., 12(9): 938-954.
8. JPT Valkonen. 2007. Viruses: economical losses and biotechnological potential. In: Vreugdenhil D, ed. Potato Biology and Biotechnology: Advances and Perspectives. Amsterdam, *Netherlands: Elsevier*, 619‑641.
9. S Gray, S DeBoer, J Lorenzen. 2010. Potato virus Y: an evolving concern for

potato crops in the United States and Canada. *Plant Disease*., 94, 1384-1397.

10. AV Karasev, SM Gray. 2013. Continuous and emerging challenges of Potato virus Y in potato. *Ann. Rev. Phy*., 51, 571-586.
11. RAC Jones. 2014. Virus disease problems facing potato industries worldwide: viruses found, climate change implications, rationalising virus strain nomenclature and addressing the Potato virus Y issue. In: Navarre R, Pavek MJ, eds. The Potato: Botany, Production and Uses. Wallingford, UK: *CABI*, 202-224.
12. C Kerlan, 2006. Potato virus Y. Descriptions of Plant Viruses, No. 414. Wellesbourne, UK: *Association of Applied Biologists*.
13. A Blanchard, M Rolland, C Lacroix, C Kerlan, E Jacquot, 2008. Potato virus Y: a century of evolution. *Cur Top Vir*. 7: 21-32.
14. C Kerlan, B Moury. 2008. Potato virus Y. In: Granoff A, Webster R, eds. Encyclopedia of Virology. 3rd edn. New York, USA: *Academic Press*, 287-296.
15. K Apel, H Hirt. 2004. Reactive oxygen species: metabolism, oxidative stress, and signal transduction. *Ann. Rev. Plant. Biol*. 55: 373-399.
16. R Mittler, S Vanderauwera, N Suzuki, G Miller, VB Tognetti, K Vandepoele, M Gollery, V Shulaev, F Van Breusegem. 2011. ROS signaling: the new wave? *Trends. Plant. Sci*. 16: 300-309.
17. CH Foyer, G Noctor. 2009. Redox regulation in photosynthetic organisms: signaling, acclimation, and practical implications. *Antioxid Redox Signal* 11: 861-905.
18. Y Xiong, AL Contento, PQ Nguyen, DC Bassham. 2007. Degradation of oxidized proteins by autophagy during oxidative stress in Arabidopsis. *Plant*

Physiol., 143: 291-299.

19. Y Liu, Y Xiong, DC Bassham. 2009. Autophagy is required for tolerance of drought and salt stress in plants. *Autophagy*. 5: 954-963.
20. ME Pérez-Pérez, FJ Florencio, JL Crespo. 2010. Inhibition of target of rapamycin signaling and stress activate autophagy in Chlamydomonas reinhardtii. *Plant Physiol.* 152: 1874-1888.
21. ME Pérez-Pérez, I Couso, JL Crespo. 2012. Carotenoid deficiency triggers autophagy in the model green alga Chlamydomonas reinhardtii. *Autophagy*. 8: 376-388.
22. C He, DJ Klionsky DJ. 2009. Regulation mechanisms and signaling pathways of autophagy. *Annu Rev Genet.* 43: 67-93.
23. N Mizushima, T Yoshimori, Y Ohsumi. 2011. The role of Atg proteins in autophagosome formation. *Annu Rev Cell Dev Biol*. 27: 107-132.
24. Y Liu, DC Bassham. 2012. Autophagy: pathways for self-eating in plant cells. *Annu Rev Plant Biol.* 63: 215-237.
25. M Tsukada, Y Ohsumi. 1993. Isolation and characterization of autophagy defective mutants of *Saccharomyces cerevisiae*. *FEBS Lett.* 333: 169-174.
26. N Mizushima, T Yoshimori, Y Ohsumi. 2011. The role of Atg proteins in autophagosome formation. *Annu Rev Cell Dev Biol.* 27: 107-132.
27. T Kirisako, Y Ichimura, H Okada, Y Kabeya, N Mizushima, T Yoshimori, M Ohsumi, T Takao, T Noda, Y Ohsumi. 2000. The reversible modification regulates the membrane-binding state of *Apg8*/*Aut7* essential for autophagy and the cytoplasm to vacuole targeting pathway. *J Cell Biol.* 151: 263-276.
28. P Dunoyer, O Voinnet. 2005. The complex interplay between plant viruses and host RNA-silencing pathways. *Curr Opin Plant Biol.* 8, 415-423.

29. F Li, SW Ding. 2006. Virus counterdefense: diverse strategies for evading the RNA-silencing immunity. *Annu Rev Microbiol.* 60, 503−531.

30. A Valli, JJ Lopez-Moya, JA Garcıa. 2009. RNA silencing and its suppressors in the plant-virus interplay. Chichester, UK: *John Wiley & Sons Ltd*.

31. P Vicente, AG Juan. 2011. How do plant viruses induce disease? Interactions and interference with host components. *J Gen Vir*. 92: 2691-2705.

32. R Christophe, C Carole. 2006. Translation initiation factors: a weak link in plant RNA virus infection. *Trend. Plant. Sci*. 11(1): 40-45.

33. H Clémence, B Véronique, ZG Véronique, R Frédéric. 2013. Viral and cellular factors involved in phloem transport of plant viruses. *Front. Plant Sci.* 24(4): 1-24.

34. JY Lee, H Lu. 2011. Plasmodesmata: the battleground against intruders., *Trend. Plant. Sci.* 16(4): 201-210.

35. L Amit, YZ Judy, GL Sondra. 2015, Synaptotagmin SYTA Forms ER-Plasma Membrane Junctions that Are Recruited to Plasmodesmata for Plant Virus Movement. *Curr Bio.,* 25(15): 2018-2025.

36. R Frédéric, AG Juan. 2015. Molecular Biology of Potyviruses. *Adv vir res*. 101-199.

37. M Sorel, JA Garcia, S German-Retana, 2014. The *Potyviridae* Cylindrical Inclusion Helicase: A Key Multipartner and Multifunctional Protein. *MPMI*. 27(3): 215-226.

38. D Riedel, DE Lesemann, E Maiß, 1998. Ultrastructural localization of nonstructural and coat proteins of 19 potyviruses using antisera to bacterially expressed proteins of plum pox potyvirus. 143: 2133-2158.

39. HO Rashid, RK Yadav, HR Kim, HJ Chae. 2015. ER stress: Autophagy

induction, inhibition and selection. *Autophagy*. 11(11): 1956-1977.

40. R Ozgur, B Uzilday, Y Iwata, N Koizumi, I Turkan. 2018. Interplay between unfolded protein response and reactive oxygen species: a dynamic duo. *J Exp Bot*. 69(14): 3333-3345.
41. C Ye, MB Dickman, SA Whitham, M Payton, J Verchot. 2011. The Unfolded Protein Response Is Triggered by a Plant Viral Movement Protein. 2011. *Plant phy*. 156: 741-755.
42. Y Bao, SH Howell. 2017. The Unfolded Protein Response Supports Plant Development and Defense as well as Responses to Abiotic Stress. *Front. Plant Sci*. 8(344): 1-6.
43. V Pallas, JA Garcia. 2011. How do plant viruses induce disease? Interactions and interference with host components. *J Gen Vir*. 92: 2691-2705.
44. B Ghoshal, H Sanfaçon. 2015. Symptom recovery in virus-infected plants: Revisiting the role of RNA silencing mechanisms. *Virology*. 479-480(2015): 167-179.
45. AA Valli, A Gallo, B Rodamilans, JJ Lopez-Moya. 2018. The HCPro from the *Potyviridae* family: an enviable multitasking Helper Component that every virus would like to have. *Mol Plant Pat*. 19(3): 744-763.
46. G Liu, Y Wu, M Xu, T Gao, P Wang, L Wang, T Guo, G Kang. 2016. Virus-Induced Gene Silencing Identifies an Important Role of the *TaRSR1* Transcription Factor in Starch Synthesis in Bread Wheat. *Int. J Mol Sci*. 17(10): 1577-1590.
47. A Ben-Shem, F Frolow, N Nelson. 2003. Crystal structure of plant photosystem I. *Nature*. 426: 630-635.
48. KH Rhee, EP Morris, J Barber, W Kühlbrandt. 1998. Three-dimensional

structure of the plant photosystem II reaction centre at 8Å resolution. *Nature*. 396: 283-286.

49. AV Ruban, M Wentworth, AE Yakushevska, J Andersson, PJ Lee, W Keegstra, JP Dekker, EJ Boekema, S Jansson, P Horton. 2003. *Nature*. 421: 648-652.
50. J Rahouteia, I Garcıa-Luqueb, M Baron. 2000. Inhibition of photosynthesis by viral infection: Effect on PSII structure and function. *Physiol Planta*. 110: 286-292.
51. JF Bol, HJM Linthorst. 1990. Plant Pathogenesis-Related Proteins Induced by Virus Infection. *Annu. Rev. Phytopathol*. 28: 113-138.
52. A Moosa, A Farzand, ST Sahi, SA Khan. 2017. Transgenic expression of antifungal pathogenesis-related proteins against phytopathogenic fungi - 15 years of success. *Isr J Plant Sci*.
53. FT Brederode, HJM Linthorst, JF Bol. 1991. Differential induction of acquired resistance and PR gene expression in tobacco by virus infection, ethephon treatment, UV light and wounding. *Plant Mol Bio*. 17: 1117-1125.

CHAPTER 2

Functional implication of autophagy in infected pepper fruits with anthracnose fungus

2.1 ABSTRACT

Colletotrichum gloeosporioides is a common pathogenic fungus in many plants including hot pepper (*Capsicum annuum*). In this study, fungal behaviours and anthracnose symptom development were compared in green and red pepper fruits. When the isolate of *C. gloeosporioides* was inoculated on both green and red fruits, conidial germination, appressoria, and infection hyphae were observed on both fruits within 24 hours after inoculation. The fungal invasion and colonization continued to the epidermal cells of green fruits, but not to those of red ones. Initial anthracnose symptoms were detected only on green fruits at 2 days after inoculation resulting in typical sunken necrosis within 5 days after inoculation. I further analyzed ROS production and antioxidant protein accumulation in the infected fruits, resulting intense oxidative stress in only green fruits followed by the HR-like cell death. To elucidate the role of autophagy, I observed the expression of ER stress-related and autophagy-related genes, representing specific induction of ER stress marker, bZIP60, in the green fruits, but not in the red fruits. The activation of UPR pathway in the green fruit was drastically attenuated

after fungal invasion into plant cells which undergo massive cell death at 72 hrous after infection. Immunolocalization results showed concurrent localization of BIP and ATG4 proteins, along with the fungal penetration in the infected region of the fruits. In addition, in response to the anthracnose fungus, the fruits displayed higher expression of PR genes, PR1 and PR10 in the green fruits and PR2 and PR3 in the red fruits, respectively. Disease symptom analysis revealed significantly low occurrence of anthracnose disease in the red fruits. These results show that fungal infection induce ER stress but suppress UPR response, leading to ER stress-induced HR-like cell death in infected green fruit.

2.2 INTRODUCTION

The name *Colletotrichum gloeosporioides* was first proposed in Penzig (1882), based on *Vermicularia gloeosporioides*, the type specimen of which was collected from *Citrus* in Italy. Much of the early literature used this name to refer to fungi associated with various diseases of *Citrus*, with other species established for morphologically similar fungi from other hosts. However, several early papers discussed the morphological similarity between many of the *Colletotrichum spp*. that had been described on the basis of host preference, and used inoculation tests to question whether or not the species were distinct. Some of these papers investigated in culture the link between the various *Colletotrichum* species and their sexual *Glomerella* state (e.g. Shear and Wood 1907, Ocfemia and Agati 1925). Authors such as Shear and Wood (1907, 1913) and Small (1926) concluded that many of the species described on the basis of host preference were in fact the same, rejecting apparent differences in host preference as a basis for taxonomic segregation. Small (1926) concluded that the names *Glomerella cingulata* and *Colletotrichum gloeosporioides* should be used for the sexual and asexual morphs, respectively, of the many *Colletotrichum* spp. they regarded as conspecific. *Colletotrichum gloeosporioides* was stated to be the earliest name with a proven link to what they regarded as a biologically diverse *G. cingulata*. The studies of von Arx and Müller (1954) and von Arx (1957, 1970) taxonomically formalised this concept (Weir, 2012).

C. gloeosporioides causes anthracnose disease on a wide variety of fruits, including almond, avocado, apple, Arabica coffee, guava, mango, strawberry,

papaya, banana, passion fruit, citrus, grapes and cashews (Simmonds, 1965, Hartill, 1992, Alahakoon, 1994, Timmer, 1998, Agwana, 1997, Freeman, 1998, Martinez-Culebras, 2000, 2003, Sanders and Korsten 2003, Xiao, 2004, Amusa, 2005, Nelson 2008). It causes considerable damage to large number of crops such as cereals, coffee, legumes (Bailey and Jeger, 1992, Lenne, 1992) and tropical, subtropical fruits such as avocado, banana, mango (Mordue, 1967, Jeffries, 1990). *Colletotrichum spp* are also found on decaying wild fruits (Tang, 2003). Under a high concentration of CO_2, there is increase in fecundity (spores produced per lesion area) observed and this may increase the severity and spread of disease (Chakraborty and Datta, 2003).

Colletotrichum species that cause serious plant disease are also commonly isolated as endophytes from healthy plants, and have been identified as saprobes on dead plant material (Photita, 2001, 2004, Promputtha, 2002, Toofanee and Dulymamode, 2002, Kumar and Hyde, 2004). The symptoms such as small, dark lesions appear on leaves, fruits and flowers of the infected plant which finally produce concentric ring pattern.

Autophagy is one of evolutionarily conserved protein degradation system in eukaryotes, by which the damaged or unnecessary proteins and cellular components are wrapped into double-membrane autophagosomes, and then delivered to the vacuole for degradation and recycling (Liu and Bassham, 2012). In the past few years, more studies about the participation of autophagy in plant response to environmental stimuli have been reported, such as oxidative (Xiong, 2007), drought, osmotic and salt (Liu et al, 2009, Kuzuoglu-Ozturk, 2012), hypoxia (Chen , 2015) and heat stress (Zhou, 2014, Zhai, 2016). The discovery of the ATG genes has greatly facilitate the progress in understanding the mechanistic basis of

autophagy, and the autophagy-related proteins that participate in autophagy process have been identified in several plant species. It is reported that 30 ATG proteins in *Arabidopsis* (Kwon and Park, 2008), 33 in rice (Xia, 2011), 31 in maize (Li, 2015), 30 in tobacco (Zhou, 2015), 29 in pepper (Zhai, 2016) and 37 in foxtail millet (Li, 2016) have been identified.

Among the ATG proteins, ATG8, an ubiquitin-like protein, is thought to play an essential role in autophagy, and has been used as a marker to monitor autophagy process (Kellner, 2017). After its precursor was cut by ATG4 from C-terminus to expose a glycine (Gly) residue and then activated by ATG7, the mature ATG8 protein is finally conjugated to the membrane phospholipid PE (phosphatidylethanolamine) to execute its function during autophagosome formation (Han. 2011). However, the contribution of ATG8 to plant tolerance to environmental stresses is ambiguous. The over-expression or heterologous of ATG8 genes from soybean, apple and foxtail millet were reported to confer the enhanced tolerance to abiotic stresses, respectively (Xia, 2012, Wang, 2016, Li, 2016). Accordingly, the silencing or mutation of ATG8 genes from *Arabidopsis* and wheat rendered the plants more sensitive to environmental stresses (Kuzuoglu-Ozturk et al., 2012, Tian et al., 2014). Nevertheless, the results of Slavikova et al. (2008) and Guo et al. (2016) showed that the tolerance of Arabidopsis to salt, osmotic and arsenic stress were weakened by the over-expression of ATG8 gene. It is therefore worthy to explore the relationship between ATG8 gene expression and plant adaption to adverse environmental conditions.

We observed the phenomena that occur when *C. annuum*. infected *C. gloeosporioides*. When infected *C. gloeosporioides*, I studied the defense mechanism in pepper. When *C. gloeosporioides* penetrates pepper fruits, autophagy

signaling works by generating ROS immediately. Pathogen-related genes also work against *C. gloeosporioides* that physically penetrate the their surface. These results suggest that the defense mechanism against phytopathogen also changes as green pepper turns into red pepper.

2.3 MATERIALS AND METHODS

2.3.1 Plant materials

Commercial pepper used in the study (*Capsicum annuum* L. cv. Nockkwang) was obtained from local conventional market (Gakhwa). Plants were grown at 25 ˚C under greenhouse conditions. Fully-grown unripe green and ripe red fruits from three-month-old pepper plants were used. The fruit was washed with tap water, washed one more time with distilled water, and then the water was removed.

2.3.2 *Colletotrichum gloeosporioides* culture and inoculation

C. gloeosporioides were cultured in potato dextrose agar at 28 ˚C. *C. gloeosporioides* cultured for 7 days were scraped with distilled water and diluted to 5×10^5 spores/ mL using a hemocytometer. 10 μL was dropped on 2－5 spots of the fruit except for both ends of the fruit. The inoculated fruit was kept in humid box at 100% humidity and cultured at 26 ˚C. Then, 0, 24, 48, 72 hpi fruits were harvested for analysis. The harvested samples were immediately frozen in liquid nitrogen.

2.3.3 Immunoblot analysis

The frozen tissues were ground using mortar with liquid nitrogen. The lysate was resuspended in 2 volumes lysis buffer (consisted of 50 mM sodium phophate (pH 7), 10 mM EDTA (ethylenediaminetetraacetic acid, pH 8), 10 mM 2-ME

(2-mercaptoethanol), 4 mM DTT (dithiothreitol), 0.1% triton X-100, 0.1% SDS (sodium dodecyl sulfate), 200 μM PMSF (phenylmethanesulfonyl fluoride), 250 mM sucrose, 10% glycerol and protein inhibitor cocktail (Sigmal Aldrich). The lysates were shaking incubated in refrigerator (4 ˚C) for 2 hours and then centrifuged at 4 ˚C. The supernatant of extracted protein was calculated using bradford assay to determine the amount of protein. The protein samples (20 μg) were heat 100 ˚C for 10 mins, separated in 12% SDS-PAGE (SDS-polyacrylamide gel electrophoresis) at 100 voltage for 90 mins at room temperature and transferred onto a polyvinylidene fluoride membrane (PVDF, 0.45 μm pore size, immobilon-FL, Merck Millipore Ltd.) for 90 mins at 4 ˚C. The membranes were blocked with 5% skim milk in TBS-T (tris-buffered saline with Tween-20) buffer for 1 hour on the shaking incubator at room temperature. The washing step was always used 3 times for 10 mins with TBS-T buffer. Primary antibody was added to membrane and shaking incubated overnight at 4 ˚C. After washing with TBS-T, the membranes were incubated with secondary antibody conjugated with peroxidase at room temperature according to the specificity of primary antibody. The blots combined with primary and secondary antibody were detected using the enhanced chemiluminescence (ECL) plus detection reagents (Claro sola, BioD Co., Ltd., Korea). Antibody informations are shown in Table 1.3.

2.3.4 Light microscopy (LM)

2.3.4.1 Fruits collection for LM

For light microscope analysis, the 0, 24, 48, 72 hpi fruits were harvested with

control fruits. The control and inoculated fruits were cut (5×5 mm^2 for paraffin embedding) and fix in 4% para-formaldehyde in 50 mM sodium phosphate buffer at pH 7.0. After segments were using for LM.

2.3.4.2 Light microscopy (LM) analysis for immunohistochemistry (IHC)

The pepper segments were performed for paraffin infiltration. For dehydration, step by step processing was carried out to following : 30－70% ethanol for 25 mins in ice on shaker, 80－100% ethanol for 25 mins at room temperature on shaker. Next, for infiltrate to paraffin, add 1:1 ethanol and chloroform (a), 100% chloroform (b), 1:1 chloroform and paraffin (c), 100% paraffin mixture (d) in order and each shake for 30 mins. (a) and (b) steps were performed at room temperature, (c) and (d) steps were performed at 65 ˚C. After overnight incubation at 65 ˚C, samples were transferred to mold for solidify. The paraffin blocks were cut into 5 μm thicknesses and attached on the slide glass at 40 ˚C. The completed samples were using for immunohistochemistry (IHC).

2.3.5 RNA extraction, cDNA synthesis and qPCR

Infected *C. gloeosporioides* pepper fruit sampels were harvested at 0, 3, 12, 24, 48 hpi. For the RNA extraction, The infected pepper fruit samples were ground using a mortar with liquid nitrogen. 1 mL of RNA extract solution (Hybrid-R™, Geneall, Korea) was added per 100 mg according to the manufacturer's instructions. The purified RNA was quantified using a UV-spectrophotometer and 1 μg of RNA was converted to cDNA using reverse transcriptase (Hyperscript™,

GeneAll). The expression of autophagy related genes, pathogen-related genes and ER stress markers in UPR pathway were confirmed by qPCR using specific primers. The qPCR was performed with a real-time thermocycler (Roter Gene-3000, Corbett research, Sydney, Australia) using the following PCR conditions: 40－60 cycles of 95 ˚C for 15 sec, 60 ˚C for 15 sec and 72 ˚C for 20 sec. Real-time PCR products were analyzed by Rotor-gene 6 program. Primer sequences are shown in Table 2.1.

Table. 2.1. *Capsicum annuum* gene-specific primers used in qPCR

Gene		Primers (5' to 3')
bZIP17-Ca-F	Forward:	GAC GGT CTT CCA GTT CCA CC (20 mers)
bZIP17-Ca-R	Reverse:	GAC CCG AGA ACA TCA GGC AA (20 mers)
bZIP60-Ca-F	Forward:	TCC CTC TGC ACC CAA TTT CC (20 mers)
bZIP60-Ca-R	Reverse:	GGC GAG TGA GAG ACC TTG TC (20 mers)
BIP3-Ca-F	Forward:	AAG ACA CGC GCT TCC TTG AC (20 mers)
BIP3-Ca-R	Reverse:	CCA TCA GTG AAG GCT ACC CA (20 mers)
DER1-Ca-F	Forward:	CCG TTG CAT GTC AGT TGG GAT (21 mers)
DER1-Ca-R	Reverse:	TCC ACT CTC CAG TTG CAC TC (20 mers)
BI1-Ca-F	Forward:	GGA GGG TTT CAC GTC GTT CT (20 mers)
BI1-Ca-R	Reverse:	CCA CAC CAT GCT TCC AAT GC (20 mers)
Ca-18S-490F	Forward:	CGG TAA TTC CAG CTC CAA TAG C (22 mers)
Ca-18S-718R	Reverse:	CCA TGC TAA TGT ATA CAG AGC GTA GG (26 mers)
PR1-Ca-F	Forward:	AAG TTG GTG TCG GCC CTA TG (20 mers)
PR1-Ca-R	Reverse:	TTG ACC CAC ATC TTC ACG GC (20 mers)
PR2-Ca-F	Forward:	GGC ACG AGA ATT ACT ATT CCT C (22 mers)
PR2-Ca-R	Reverse:	GGT GGC AGC AAT GTT TTG AAG A (22 mers)

2.4 RESULTS

2.4.1 Cultivation of *C. gloeosporioides* for inoculation of pepper fruit

C. gloeosporioides subcultured in potato dextrose agar (PDA). The matured *C. gloeosporioides* was slightly orangeish and grayish and fluffy. *C. gloeosporioides* was used to spread throughout the plate when cultured at 28 ˚C for 7 days. C. *gloeosporioides* was diluted to 5×10^5 spores per μL in distilled water. 10 μL (5,000 spores) were inoculated on cover glass and incubated at 26 ˚C for 24 hours. After 24 hours, germination and appressorium morphology were observed. *C. gloeosporioides* was 90% germination and 70% of them had appressorium (Fig 2.1). Appressorium was observed in a round shape under a microscope, but some forms were irregular. The length of the hyphae was very short. *C. gloeosporioides* was inoculated with 5,000 spores in healthy red and green pepper. The inoculated peppers were placed in a humid box and incubated at 26 ˚C. The fruits were removed from the incubator after 10 days and observed for symptoms. In the case of green pepper, infection was caused by *C. gloeosporioides*, but no infection occurred in red pepper (Fig 2.2).

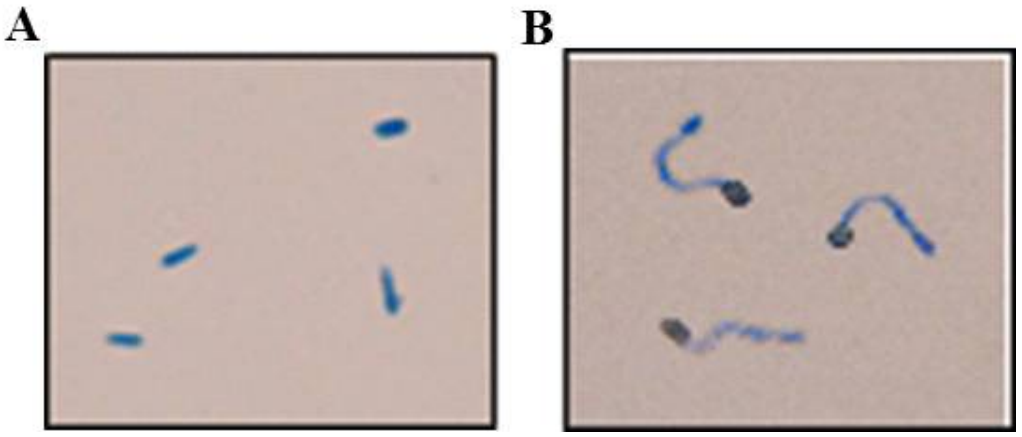

Figure 2.1. *In vitro* germination and appressorium formation of *C. gloeosporioides*. *C. gloeosporioides* on cover glass in 24 hour culture. The fungus attaches to the fruit surface and then forms an appressorium. Appressorium is used to physically penetrate the surface of the pepper fruit.

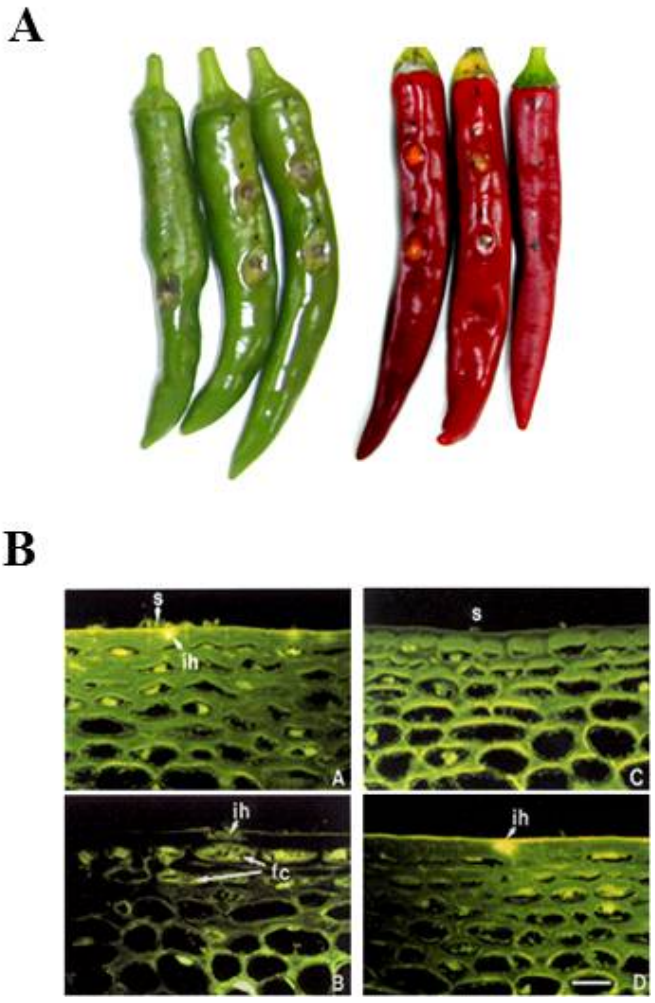

Figure 2.2. Disease development on the unripe green and the ripe red fruits infected with *Colletotrichum gloeosporioides*. A, Representative photographs of infected pepper fruits challenged with *C. gloeosporioides*. B, Microscopic observation of fungal penetration at the infection area in the unripe and the ripe fruits infected with *C. gloeosporioides*. a. unripe fruit at 48 hpi; b, unripe fruit at 72 hpi; c, ripe fruit, at 48 dpi; d, ripe fruit, at 72 dpi.

2.4.2 *C. gloeosporioides* invasion into the fruits and response the cell according to accumulate of ROS generation

The pepper fruits turn from green pepper to red pepper over time. Infection with *C. gloeosporioides* begins by attaching to the surface of the pepper fruit. After attachment, it penetrates through plant cell walls using appressorium. The plant detects *C. gloeosporioides* penetration and activates the ROS generation and defense system. As pepper fruits progress to ripening, antioxidant activity increases and superoxide level decreases (Fig 2.2.A). In addition, the infection rate of *C. gloeosporioides* was remarkably decreased as ripening proceeded. As spore attachment ability decreased, disease did not develop as ripening progressed. The size of lesions due to *C. gloeosporioides* infection decreased as the developmental stage progressed (Fig 2.2.B). As a result, the antioxidant activity increases and the infection rate of *C. gloeosporioides* decreases as the green pepper is changed to red pepper.

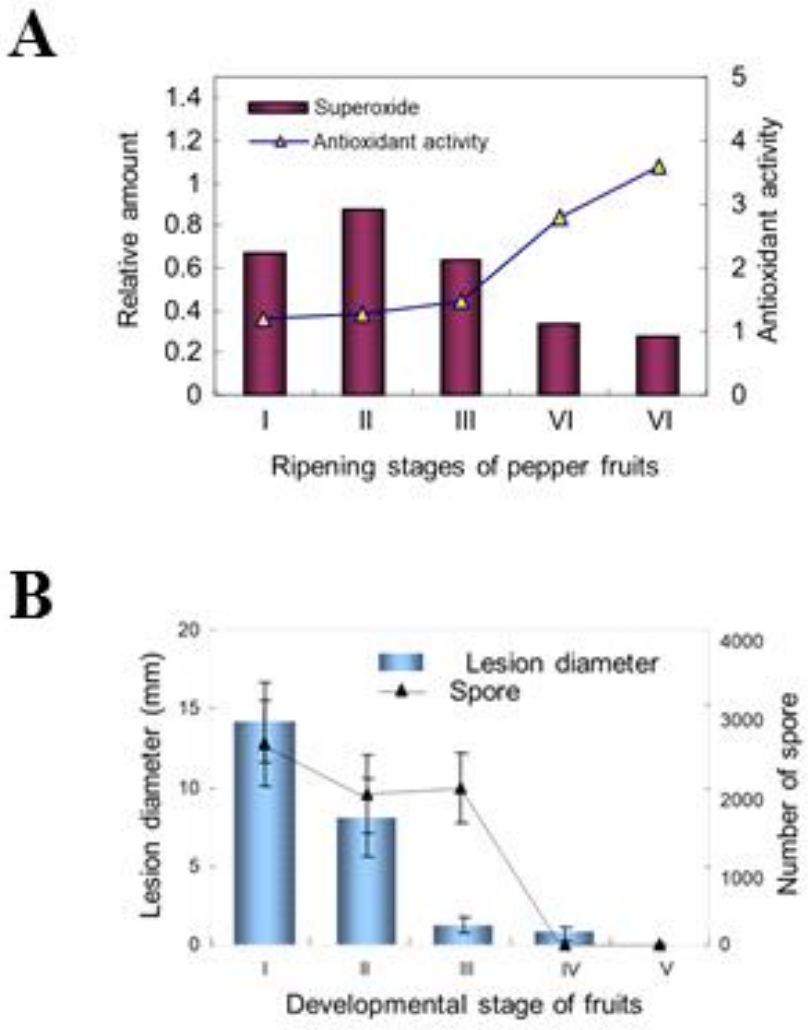

Figure 2.3. Ripening dependent antioxidant activity in the fruits of *Capsicum annuum* showing different disease severity by anthracnose fungus. (A) antioxidant activity and superoxide generation during the ripening stages of pepper fruits. (B) Lesion diameter caused by *C. gloeosporioides* on pepper fruits at five different ripening stages. I, green fruit; Ⅱ; Ⅲ; Ⅳ; Ⅴ; red fruit.

2.4.3 Identification of ROS in *C. gloeosporioides* infection by NBT and DAB staining

C. gloeosporioides infection causes ROS in pepper fruit. The surface of pepper fruits infected with *C. gloeosporioides* was observed at 0 and 24 hours after infection. During the infection of *C. gloeosporioides*, the presence of ROS was observed according to the development stage of the fruit. NBT staining at 0 hour of *C. gloeosporioides* infection showed spores on some surfaces but no accumulation of superoxide (O_2-). When NBT staining was performed after 24 hours, superoxide accumulation was observed in the epidermal cells of green fruit. However, accumulation of superoxide was not observed in red fruit (Fig 2.3.A). The accumulation of hydrogen peroxide (H_2O_2) produced by *C. gloeosporioides* infection was observed. Observation of the surface of green and red fruits at 0, 24 hours after infection with *C. gloeosporioides* through DAB staining revealed accumulation of hydrogen peroxide in the green fruit. (Fig 2.3.B). But the accumulation of hydrogen peroxide was not observed in the case of red fruit through DAB staining.

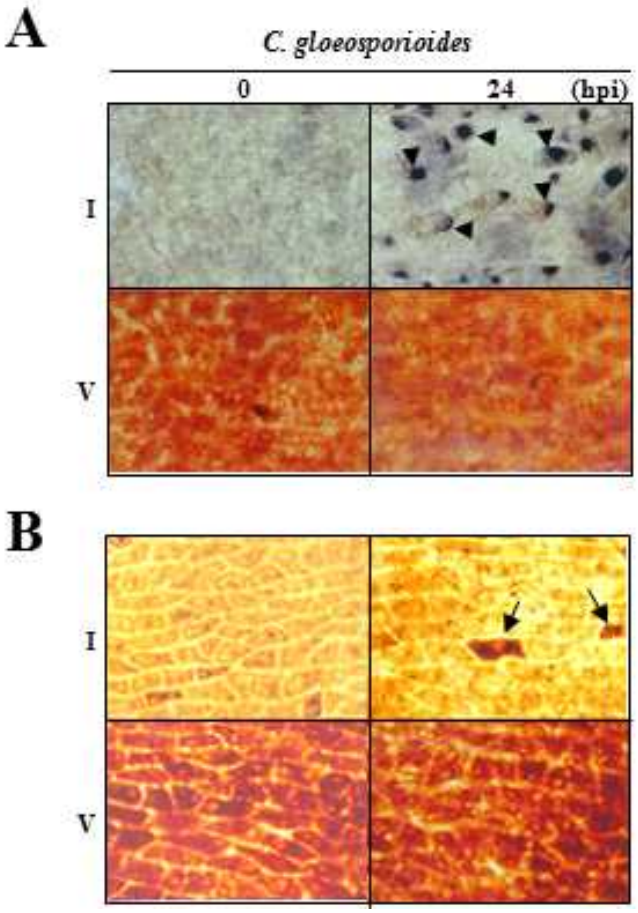

Figure 2.4. Generation of superoxide and hydrogen peroxide in the epidermis of unripe and ripe pepper fruits after fungal infection. (A) NBT staining was performed to detect superoxide generation in the unripe and the ripe fruits infected with *Colletotrichum gloeosporioides*. Arrow heads indicate NBT precipitation by superoxide. (B) DAB staining was performed to detect hydrogen peroxide in unripe and ripe fruits infected with *Colletotrichum gloeosporioides*, at 24 hours post inoculation (hpi). Arrow indicate the accumulation of hydrogen peroxide. I, fruit stage I representing unripe mature green fruit; V, fruit stage V, representing the ripe red fruit.

2.4.4 SDS-PAGE and western blot analysis for defense mechanisms of green and red pepper with *C. gloeosporioides* infection

There was a difference in the amount of ROS produced by *C. gloeosporioides* infection of Green fruit and Red fruit. Western blotting was performed to confirm the effect of antioxidant enzyme. Infected pepper fruits of 0, 24, 48, 72 hpi were used for western blot. In Fig 2.4, the FeSOD level, a chloroplastic enzyme, was higher in red fruit than in green fruit. On the other hand, mitochondrial enzyme MnSOD decreased in red fruit. Another chloroplastic ennzyme, Cu/ZnSOD, was also highly expressed in red fruit. Ascorbate peroxidase was highly expressed in red fruit and showed high expression even at 0 hour. Catalase, like APX, showed high expression in red fruit. Overall, red fruit exhibits high ROS scavenging enzyme activity in a shorter time than green fruit.

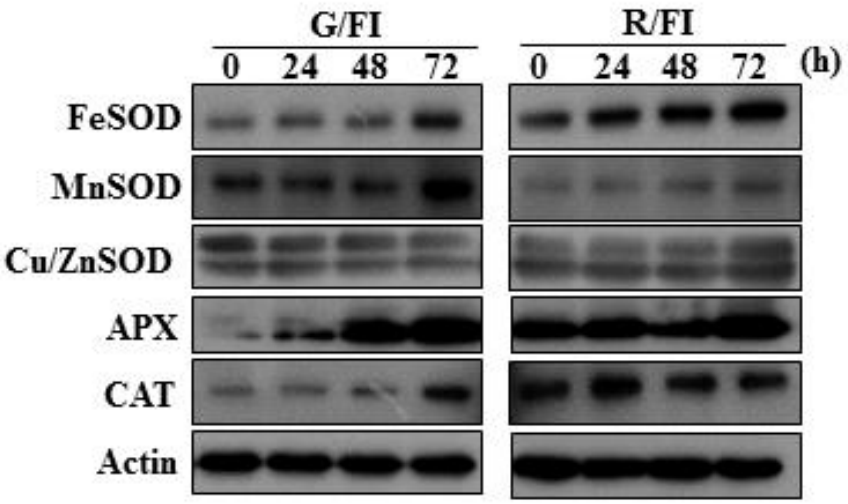

Figure 2.5. Fungal induced expression of antioxidant enzymes in unripe green fruit and ripe red fruit of *Capsicum annuum* infected with *Colletotrichum gloeosporioides*. The numbers are incubation time after fungal infection indicated time, represented as hours post inoculation (hpi). FeSOD, Chloroplastic Fe-dependent superoxide dismutase; MnSOD, Mitochondrial manganese superoxide dismutase; Cu/ZnSOD, Chloroplast copper/zinc superoxide dismutase; APX, Ascorbate peroxidase; CAT, Catalse. Protein extracts were prepared from infected fruits for Western blot analysis to determine the levels of protein accumulation. Actin was used as loading control.

2.4.5 Monitoring ER stress-related and Autophagy-related genes in infected fruits

The anthracnose fungus, *Colletotrichum gloeosporioides*, was previously shown to have an incompatible interaction with ripe-red fruit of pepper (*Capsicum annuum*). However, the fungus had a compatible interaction with unripe mature-green fruit. Using immunoblot analysis, we characterized autophagy-related genes expressed in the incompatible and compatible interactions. The ATG4 gene encodes a cysteine protease protein that is essential to autophagy and regulates autophagy through the processing of ATG8. In this experiment, the expression level of ATG4 was higher in the healthy pepper fruits regardless of the ripening stages and then slightly decreased by fungal infection in both unripe and ripe fruits. Meanwhile, lipidated ATG8 protein was constitutively accumulated in the healthy fruits. The induction of ATG8 protein was weakly up-regulated in both fruits by fungal infection. The expression level of ATG8 was much higher in the unripe green fruits compare to that of ripe red fruits. In addition, we observed the expression of ER Chaperone, BiP, to monitor endoplasmic reticulum stress in infected pepper fruits. Bip protein was consistently accumulated in the mature fruits and remained the intensity through the experimental period in both unripe and ripe fruits.

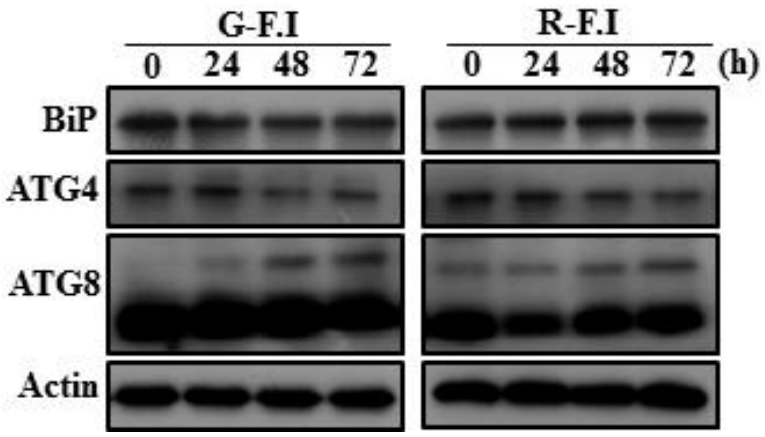

Figure 2.6. Fungal induced expression of Autophagy related protein in unripe green fruit and ripe red fruit of *Capsicum annuum* infected with *Colletotrichum gloeosporioides*. The numbers are incubation time after fungal infection, represented as hours post inoculation (hpi). BiP2, lumenal-binding protein; ATG4, autophagy protein 4; ATG8, autophagy protein 8; Protein extracts were prepared from infected fruits for Western blot analysis to determine the levels of protein accumulation. Actin was used as loading control.

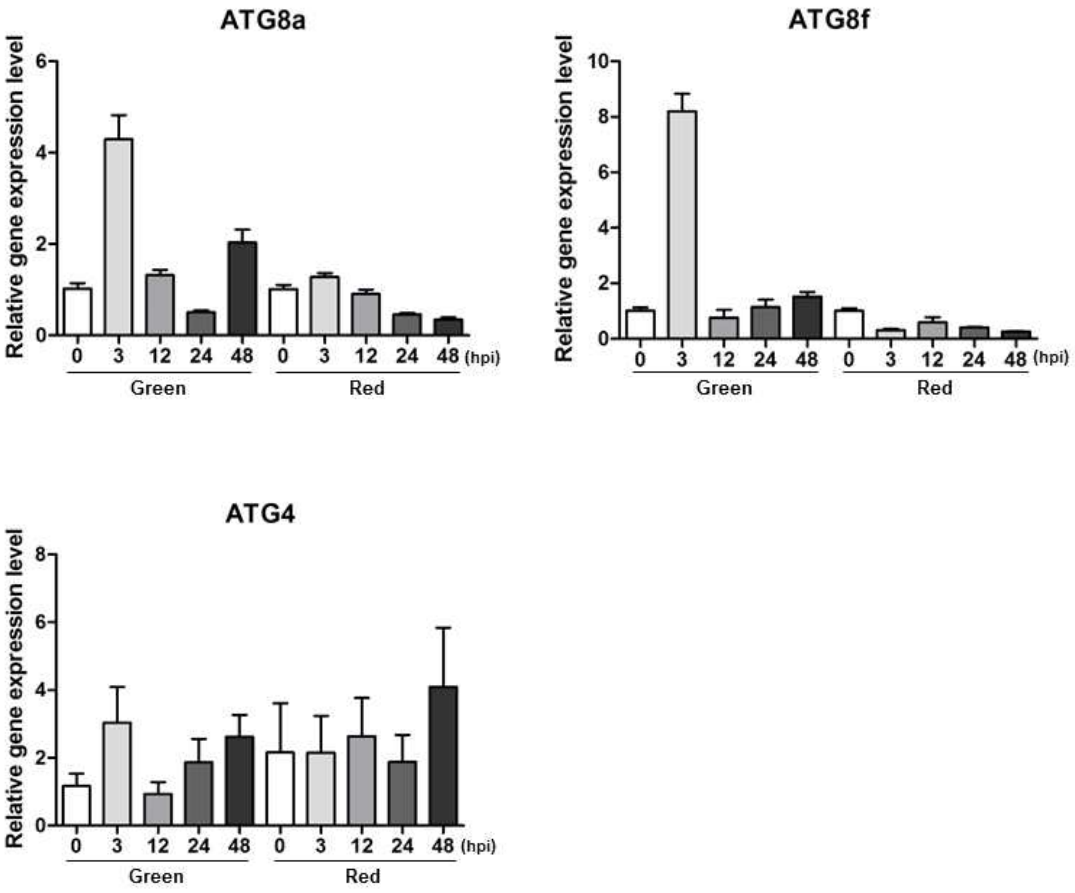

Figure 2.7. Expression level of autophagy component genes in green and red fruits after *C. gloeosporioides* infection. *C. g* infected pepper fruits samples (green and red fruits) were harvested at 0, 3, 12, 24, 48 hpi. *ATG4*, *ATG8a* and *ATG8f* were confirmed expression levels using qPCR. Data shown represent fold changes of genes and display the ratio of housekeeping gene *18S* using the $^{\Delta\Delta}$Ct analyze method.

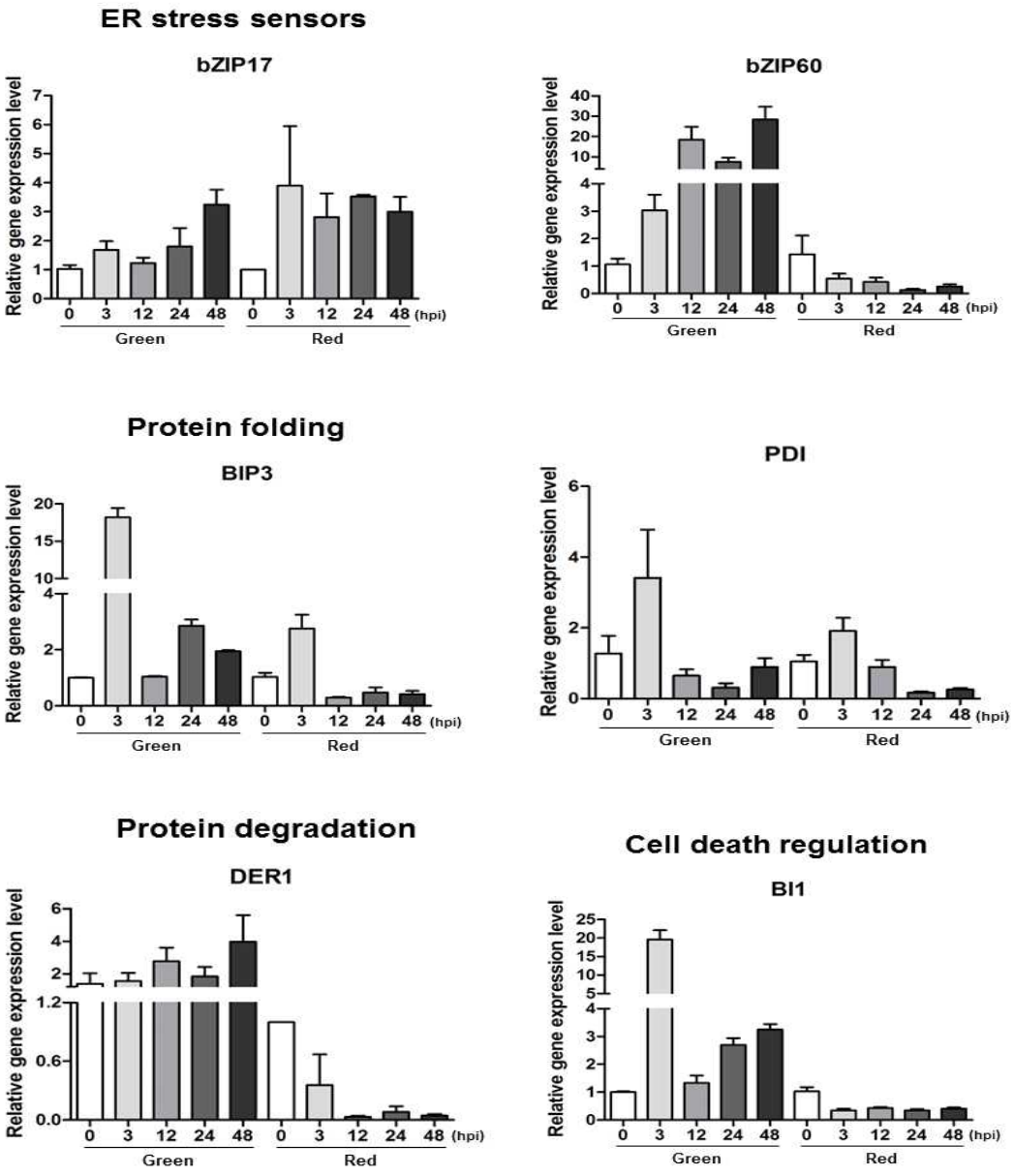

Figure 2.8. Expression level of UPR pathway components in green and red fruits after *C. gloeosporioides* infection. 0, 3, 12, 24, 48 hpi *C. gloeosporioides* infected fruits were harvested. ER stress sensors marker genes, *bZIP17* and *bZIP60*, protein folding marker genes, *BiP3* and *PDI*, protein degradation marker, *DER1*, cell death regulation marker, *Bax inhibitor-1*(*BI-1*), were confirmed expression levels using qPCR. Data shown represent fold changes of genes and display the ratio of housekeeping gene *18S* using the $^{\Delta\Delta}$Ct analyze method.

2.4.6 Localization of ER stress marker and ATG4 protein in infected fruits

Analysis of BiP accumulation by in situ immunolocalization showed that the accumulation of BiP was localized in the epidermal cells and subepidermal cells, but less in the cortical cell layers. An examination of transverse sections of the fruits inoculated with the fungus showed that the fungus invaded and colonized some epidermal cells of the unripe fruit at 24 and 72 hours after inoculation, respectively, but not those of the ripe fruit. However, BiP proteins were preferentially localized in the epidermal cells in both unripe and ripe fruits by fungal infection. These results suggest that the ER stress take part in the fruits development. On both unripe and ripe fruits, when the fungus tried to invade, the ER stress was increased in the epidermal cells that was directly contact with the fungus. Additionally, the ATG4 protein was randomly detected in the surface area of the fruits in both unripe and ripe fruits. By fungal infection, fungal-colonized epidermal cells showed intense ATG4 accumulation in infected unripe fruits, but not in the ripe fruits.

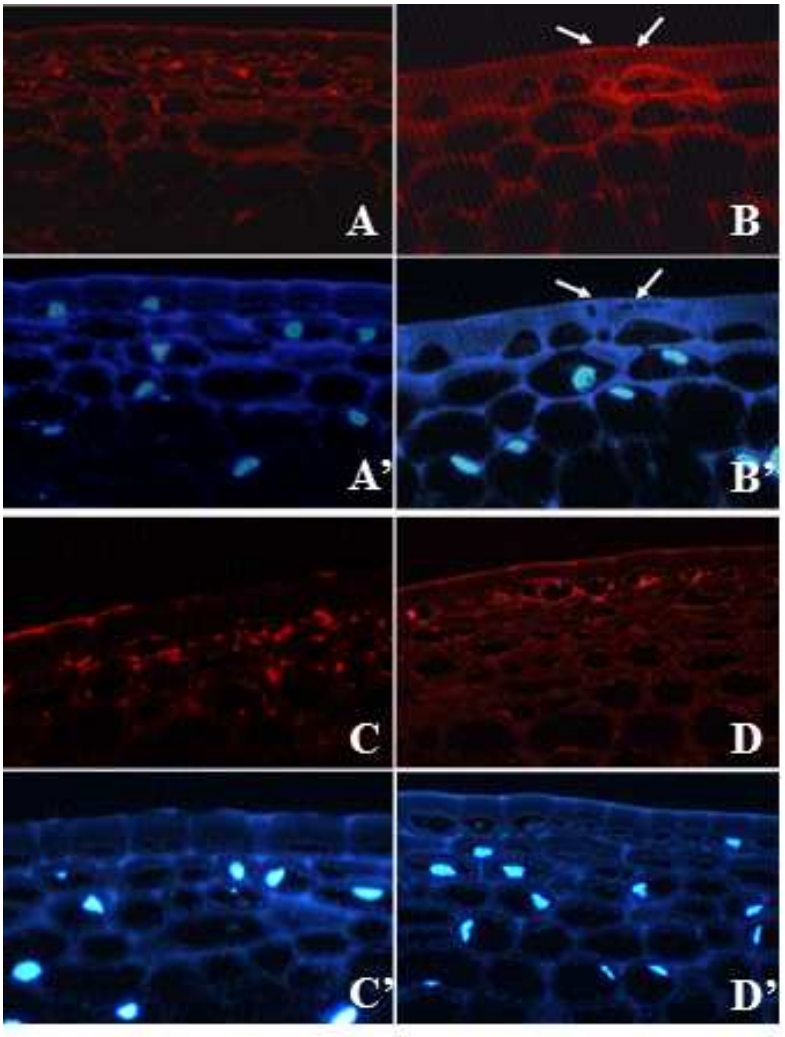

Figure 2.9. Immunolocalization of BIP in the unripe and ripe fruits of *Capsicum annuum* infected with *Colletotrichum gloeosporioides*. **(A)** Unripe pepper fruits before fungal infection. **(A')** DAPI stain of **A**. **(B)** Unripe pepper fruits at 72 hpi. **(B')** DAPI stain of **B**. **(C)** Ripe pepper fruits before fungal infection. **(C')** DAPI stain of **C**. **(D)** Ripe pepper fruits at 72 hpi. **(D')** DAPI stain of **D**.

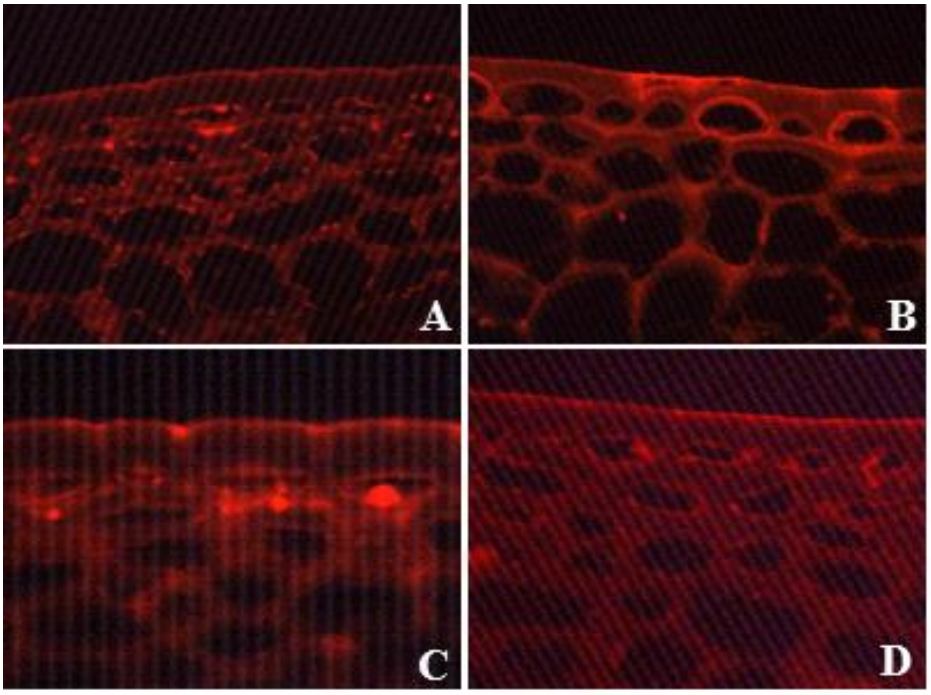

Figure 2.10. Immunolocalization of ATG4 in the unripe and ripe fruits of *Capsicum annuum* infected with *Colletotrichum gloeosporioides*. **(A)** Unripe pepper fruits before fungal infection. **(B)** Unripe pepper fruits at 72 hpi. **(C)** Ripe pepper fruits before fungal infection. **(D)** Ripe pepper fruits at 72 hpi.

2.4.7 Expression of pathogen-related proteins in infected fruits

Plants have evolved several defense mechanisms in response to biotic stress. The responses involve the transcriptional activation of a specific set of defense-related genes, including pathogenesis-related (PR) genes that encode mostly small proteins with anti-microbial activity (Fu and Dong, 2013). Several PR genes have been identified as markers for the defense responses of pepper to pathogen infection, which include chitinase (PR3) and ribonuclease-like protein (PR10). In a gel blot analysis of the soluble protein fraction of pepper fruits infected with the anthracnose fungus. The results showed that expression of PR3 was induced in both fruits after fungal infection. The fungal induced expression of PR3 protein was much higher in the ripe fruits. Even more the basal level of PR3 was observed in the ripe fruits. On the other hand, the anti-PR10 antibody specifically recognized two protein bands including the predicted molecular mass of PR10, as well as higher-molecular-weight proteins. The expression level of PR10 was much higher in the unripe fruits compare to that of ripe fruits. These results suggest that fungal infection on the fruits may lead to a potentiated state for disease resistance in pepper cells by increasing defense related genes.

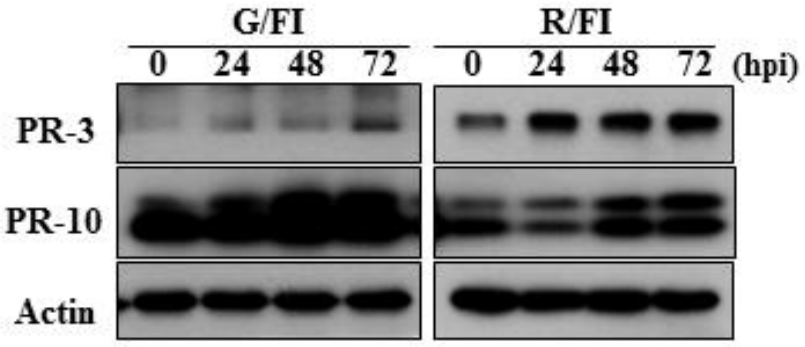

Figure 2.11. Fungal induced expression of pathogenesis related protein in unripe green fruit and ripe red fruit of *Capsicum annuum* infected with *Colletotrichum gloeosporioides*. The numbers are incubation time after fungal infection, represented as hours post inoculation (hpi). PR-3, pathogenesis-related protein 3; PR-10, pathogenesis-related protein 10. Protein extracts were prepared from infected fruits for Western blot analysis to determine the levels of protein accumulation. Actin was used as loading control.

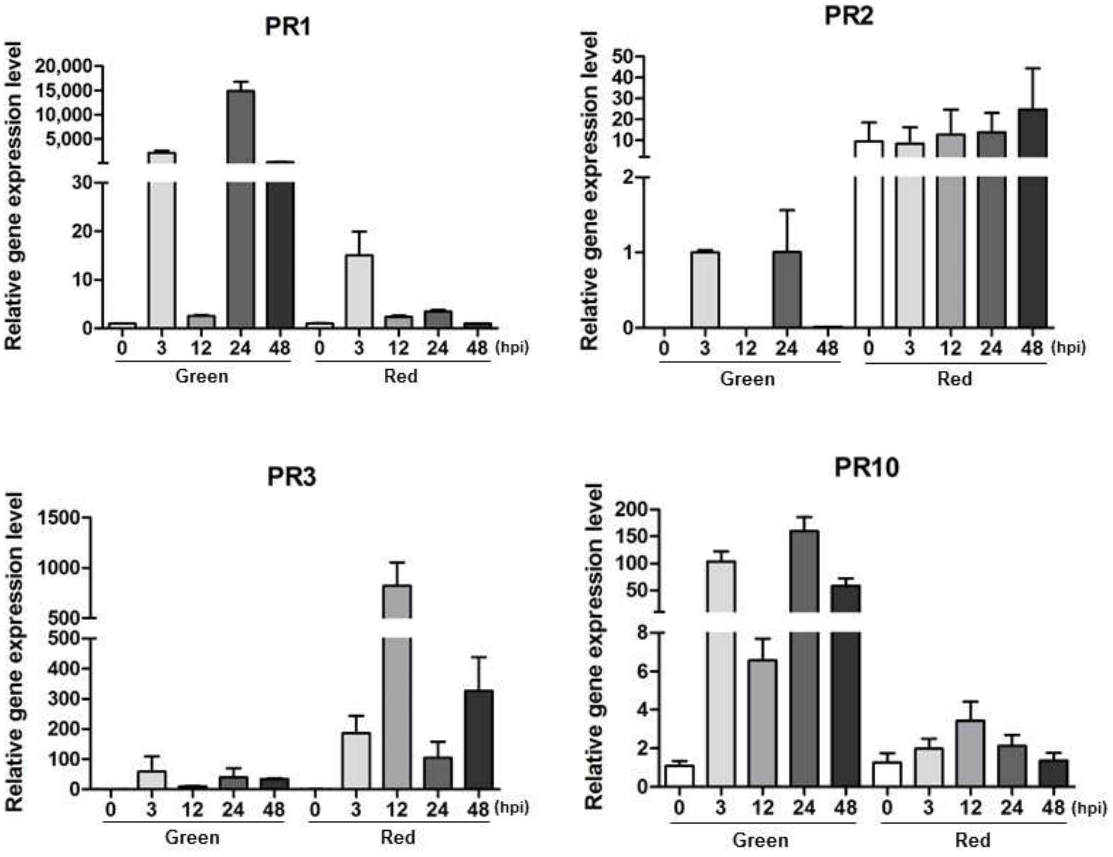

Figure 2.12. Expression level of pathogen-related genes in green and red fruits after *C. gloeosporioides* infection. *C. gloeosporioides* infected pepper fruits samples (green and red fruits) were harvested at 0, 3, 12, 24, 48 hpi. Salicylic acid and jasmonic acid based on pathogen-related genes, *PR1*, *PR2*, *PR3*, *PR10* were confirmed expression levels using qPCR. Data shown represent fold changes of genes and display the ratio of housekeeping gene *18S* using the $^{\Delta\Delta}$Ct analyze method.

2.5 DISCUSSION

Relationships between cuticular wax and disease resistance have been found in many host-pathogen systems, different strains of *C. gloeosporioides* cause anthracnose on green and red pepper fruits (Kim et al, 1986; Park and Kim 1992; Manandhar et al, 1995a, b). A recent study by the present authors (Kim et al., 1997; Oh et al., 1998) showed that the isolate KG13 of *C. gloeosporioides* caused anthracnose symptoms on green fruits only. Oh et al. (1998) reported that the specific infection of green fruits by the isolate may be due to successful colonization of the epidermal cells through cuticular layers of green pepper fruits. It has been suspected that the cuticular wax layers of pepper fruits may be related with the specific infection of green and red fruits by the isolate. Man andhar et al. (1995a) reported that cuticle thickness of pepper fruits was negatively correlated with conidial production of *C. gloeosporioides*, but not anthracnose lesion expansion. In this study, larger lesions and more conidia on wax-removed red fruits, but not green ones, compared with controls strongly indicate that the cuticular wax layer of the incompatible red fruits plays an important role in preventing fungal infection. This may also be supported by the observation that pin-pricked red fruits allowed the conidia easy access into fresh tissues and resulted in significantly larger lesions with more conidia than wax-removed fruits.

The infection of *C. gloeosporioides* is achieved through conidial germination, appressoria formation, and infection hyphae formation which are necessary for subsequent cuticular penetration (Bailey et al., 1992). In our microscopic

observations although about 70 to 90% initial infection hyphae were found on wax-removed red fruits, they failed to produce typical anthracnose lesions. Interestingly, only 20% infection hyphae formed on untreated green fruits but they caused typical anthracnose symptoms. These data imply that the isolate failed to continue colonization of the incompatible red fruit tissues, but not on the compatible green ones. The unsuccessful infection of red fruits by the isolate may be due to a failure to produce the necessary enzymes. This speculation may be supported by the facts that typical anthracnose symptoms by *Colletotrichum* species on many host plants involve the death and maceration of infected host tissues (Bailey et al., 1992). Additionally, the symptoms have been related with the production of polygalacturonases, pectin lyases and other enzymes by *Colletotrichum* species (Bailey et al., 1992; Podila et al., 1995; Wattad et al., 1997).

Leachates of fruits and leaves enhanced the conidial germination and appressorium formation in *Colletotrichum* species (Adikaram et al., 1983). Manandhar et al. (1995c) suspected that the removal of the surface wax by dipping in chloroform may afect the cutin, pectin, and cellulose components of the cuticle, resulting in more nutrients permeating from the epidermis[Increased germination, appressorium formation, and infection hyphae formation on wax-removed red fruits may have resulted from the release of various soluble compounds produced by the disrupted epidermal cells following chloroform treatment as shown in the histological study.

The difference in susceptibility of green and red fruits with *C. gloeosporioides* isolate KG02 may also be due to biochemical differences in the fruits[In biochemical analysis of peppers, green fruits had higher activities in peroxidase

and polyphenoloxidase than red fruits, but had lower levels of total phenolic substances, reducing sugars, total carbohydrates, and amino acids, some of which have been reported in relation to host resistance (Ko, 1986, Park et al., 1989). Furthermore, red fruits had 37 kDa and 22 kDa glycoproteins, whereas green fruits had only the 37 kDa glycoprotein (Park et al., 1989). These glycoproteins have been known to be important molecules in cell recognition processes between hosts and pathogens (Albersheim and Anderson-Prouty, 1975; Keen and Legrand 1980).

Although all ages of pepper fruits were susceptible to infection by *C. g loeosporioides* purple and ripe red fruits developed more anthracnose than the less developed stages of fruits (Manandhar et al., 1995c). Stockwell and Hanchey (1985) showed that cuticles of bean hypocotyls (more than 3 weeks old) were a barrier to infection by *Rhizoctonia solani*.

2.6 REFERENCES

1. BS Weir, PR Johnston, U Damm. 2012. The *Colletotrichum gloeosporioides* species complex. *Stu Myc*. 73: 115-180
2. AGO Penzig. 1882. Fungi agrumicoli. *Contribuzione* allo studio dei funghi parassiti degli agrumi. *Michelia* 2: 385.508
3. BC Sutton, JM Waterston. 1970. *Colletotrichum musae*. *CMI Descriptions of Plant Pathogenic Fungi and Bacteria*. No. 222.
4. GO Ocfemia, JA Agati. 1925. The cause of anthracnose of avocado, mango and upo in the Philippine Islands. *Philippine Agriculturalist*. 14: 199.216.
5. PV Martinez-Culebras, E Barrio, MD Garcia, A Querol. 2000. Identification of *Colletotrichum* species responsible for anthracnose of strawberry based on the internal transcribed spacers of the ribosomal region. *FEMS Microbiology Letters.* 189: 97-101.
6. PV Martinez-Culebras, A Querol, MB Suarez-Fernandez, MD Garcia-Lopez, E Barrio. 2003. Phylogenetic relationships among *Colletotrichum* pathogens of strawberry and design of PCR primers for their identification. *Journal of Phytopathology.* 151: 135-143.
7. M Maymon, A Zveibil, S Pivonia, D Minz, S Freeman. 2006. Identification and characterisation of benomyl-resistant and sensitive populations of *Colletotrichum gloeosporioides* from statice (Limonium spp.). *Phytopathology.* 96: 542-548.
8. PR Mills, S Sreenivasaprasad, AE Brown. 1992. Detection and differentiation of *Colletotrichum gl Maymon oeosporioides* isolates using PCR. *FEMS*

Microbiological Letters. 98: 137-144.

9. AK Misra. 2004. Guava diseases their symptoms, causes and management. In: Diseases of fruits and vegetables. Diagnosis and management Volume 2. (Naqvi SAMH. ed.). *Kluwer Academic Publishers*, Dordrecht: 81-119.
10. JEM Mordue. 1971. *Glomerella cingulata*. CMI Desriptions of Plant Pathogenic Fungi No. 315. *Commonwealth Mycological Institute*, Kew.
11. J Moriwaki, T Sato, T Tsukiboshi. 2003. Morphological and molecular characterisation of *Colletotrichum boninense* sp. nov. from Japan. *Mycoscience.* 44: 47-53.
12. J Moriwaki, T Sato. 2009. A new combination for the causal agent of tea anthracnose: Discula theae-sinensis (I. Miyake) Moriwaki & Toy. Sato, comb. nov. *Journal of General Plant Pathology*. 75: 359-361.
13. J Moriwaki, T Tsukiboshi. 2009. *Colletotrichum echinochloae,* a new species on Japanese barnyard millet (Echinochloa utilis). *Mycoscience.* 50: 273-280.
14. F Munaut, N Hamaide, H Maraite. 2002. Genomic and pathogenic diversity in *Colletotrichum gloeosporioides* from wild native Mexican *Stylosanthes* spp., and taxonomic implications. *Mycological Research.* 106: 579-593.
15. F Munaut, N Hamaide, J Vander Stappen, H Maraite. 1998. Genetic relationships among isolates of *Colletotrichum gloeosporioides* from *Stylosanthes* spp. in Africa and Australia using RAPD and ribosomal DNA markers. *Plant Pathology.* 47: 641-648.
16. N Muraleedharan, UI Baby. 2007. Tea disease: ecology and control. In: Encyclopedia of Pest Management Vol. 2 (Pimentel D, ed.) [electronic resource]. *CRC Press*, Boca Raton: 668-671.
17. RH Nilsson, M Ryberg, E Kristiansson, K Abarenkov, KH Larsson. 2006.

Taxonomic reliability of DNA sequences in public sequence databases: a fungal perspective. *PLoS ONE.* 1(1): e59.

18. HI Nirenberg, U Feiler, G Hagedorn. 2002. Description of *Colletotrichum lupini comb*. nov. in modern terms. *Mycologia*. 94: 307-320.
19. F Noak. 1901. Die Krankheiten des Kaffeebaumes in Brasilien. Zeitschrift f Pflanzenkrankheiten. 11: 196-203.
20. GO Ocfemia, JA Agati. 1925. The cause of anthracnose of avocado, mango and upo in the Philippine Islands. *Philippine Agriculturalist.* 14: 199-216.
21. OK Donnell, E Cigelnik. 1997. Two divergent intragenomic rDNA ITS2 types within a monophyletic lineage of the fungus Fusarium are nonorthologous. *MoIecular Phylogenetics and Evolution.* 7: 103-116.
22. OK Donnell, HI Nirenberg, T Aoki, E Cigelnik. 2000. A Multigene phylogeny of the *Gibberella fujikuroi* species complex: Detection of additional phylogenetically distinct species. *Mycoscience.* 41: 61-78.
23. OF Owolade, AGO Dixon, BS Alabi, SR Akande, SA Olakojo. 2008. A combining ability analysis of cassava *Manihot esculenta* Crantz genotypes to anthracnose disease. Electronic Journal of Environmental, *Agricultural and Food Chemistry*. 7: 2959-2968.
24. S Parvin, OR Lee, G Sathiyaraj, A Khorolragchaa, YJ Kim. 2012. Interrelationship between calmodulin (CaM) and H_2O_2 in abscisic acid-induced antioxidant defense in the seedlings of Panax ginseng. *Molecular Biology Reports*. 39: 7327-7338.
25. AGO Penzig. 1882. Fungi agrumicoli. Contribuzione allo studio dei funghi parassiti degli agrumi. *Michelia* 2: 385-508.
26. S Phoulivong, CLN Parinn, H Chen, K Abd-Elsalam. 2011. A new species of

Colletotrichum from Cordyline fruticosa and Eugenia javanica causing anthracnose disease. *Mycotaxon*. 114: 247-257.

27. JJ Polashock, FL Caruso, PV Oudemans, PS McManus, JA Crouch. 2009. The North American cranberry fruit rot fungal community: a systematic overview using morphological and phylogenetic af.nities. *Plant Pathology*. 58: 1116-1127.
28. G Pollacci. 1899. Contribuzione alla micologia ligustica. Atti dell□Istituto Botanicodell□Universitdi Pavia, Serie 2(5): 29-46.
29. D Posada. 2008. JModelTest: Phylogenetic Model Averaging. *Molecular Biology and Evolution* 25: 1253-1256.
30. N Prasad, RD Singh. 1960. Anthracnose disease of *Dioscorea alata* L. (Yam, Eng., Ratalu, Hind.). *Current Science*. 29: 66-67.
31. H Prihastuti, L Cai, H Chen, EHC McKenzie, KD Hyde. 2009. Characterisation of *Colletotrichum* species associated with coffee berries in northern Thailand. *Fungal Diversity*. 39: 89-109.
32. CJ Rodrigues, VMP Varzea, H Hindorf, EF Medeiros. 1991. Strains of *Colletotrichum coffeanum Noack* causing coffee berry disease in Angola and Malawi with characteristics different to the Kenya strain. *Journal of Phytopathology*. 131: 205-209.
34. RJ Rodriguez, JL Owen. 1992. Isolation of Glomerella musae [teleomorph of *Colletotrichum musae* (Berk. & Curt.) Arx] and segregation analysis of ascospore progeny. *Experimental Mycology*.16: 291-301.
35. Z Maldonado. 2005. Heterothallic mating observed between Mexican isolates of Glomerella lindemuthiana. *Mycologia*.97: 793-803.
36. EI Rojas, SA Rehner, GJ Samuels, SAV Bael, EA Herre. 2010. *Colletotrichum gloeosporioides* associated with *Theobroma cacao* and other plants in *Panam*

multilocus phylogenies distinguish host-associated pathogens from asymptomatic endophytes. *Mycologia.* 102: 1318-1338.

37. GM Sanders, L Korsten. 2003. Comparison of cross inoculation potential of South African avocado and mango isolates of *Colletotrichum gloeosporioides. Microbiological Research.* 158: 143-150.
38. CL Schoch, KA Seifert, S Huhndorf, V Robert, JL Spouge. 2012. Nuclear ribosomal internal transcribed spacer (ITS) region as a universal DNA barcode marker for Fungi. *Proceedings of the National Academy of Sciences.* 109: 6241-6246.
39. CL Shear, AK Wood. 1907. Ascogenous forms of Gloeosporium and *Colletotrichum*. *Botanical Gazette.* 43: 259-266.
40. BD Shenoy, R Jeewon, WH Lam, DJ Bhat, PP Than. 2007. Morpho-molecular characterisation and epitypification of *Colletotrichum capsici* (*Glomerellaceae*, *Sordariomycetes*), the causative agent of anthracnose on chilli. *Fungal Diversity*. 27: 197-211.
41. DN Silva, P Talhinhas, CLL Manuel, EK Gichuru. 2012. Host-jump drives rapid and recent ecological speciation of the emergent fungal pathogen *Colletotrichum kahawae*. *Molecular Ecology.* 21: 2655-2670.
42. R Silva-Mann, MGGV Carvalho, JC Machado, FJR Bernandino, KCC Salgado, MR Stevens. 2005. AFLP markers differentiate isolates of *Colletotrichum gossypii* from *C. gossyp*ii var. cephalosporioides. *Fitopatologia Brasileira* 30: 169-172.
43. BJ Oh, KD Kim, YS Kim. 1999. Effect of Cuticular Wax Layers of Green and Red Pepper Fruits on Infection by *Colletotrichum gloeosporioides*. *J Phytopatho*. 147: 547-552.

44. YS Kim, HH Lee, MK Ko, CE Song, CY Bae, YH Lee, BJ Oh. 2001. Inhibition of Fungal Appressorium Formation by Pepper (*Capsicum annuum*) Esterase. *Am Phytopatho Soc*. 14(1): 80-85.

45. KH Kim, JB Yoon, HG Park, EW Park, YH Kim. 2004. Structural Modifications and Programmed Cell Death of Chili Pepper Fruit Related to Resistance Responses to *Colletotrichum gloeosporioides* Infection. *Am Phytopatho Soc*. 94(12): 1295-1305.

46. SK Park, AR Park, SD Im, YJ Han, SB Lee, KW Back, JI Kim, YS Kim. 2014. Developmentally Regulated Sesquiterpene Production Confers Resistance to *Colletotrichum gloeosporioides* in Ripe Pepper Fruits. *Plos One*. 9(10): 1-10.

47. A Moosa, A Farzand, ST Sahi, SA Khan. 2017. Transgenic expression of antifungal pathogenesisrelated proteins against phytopathogenic fungi − 15 years of success. *Isr J Plant Sci.*

48. G ana, F Joana, SS Marta, F Andreia. 2016. Linking Jasmonic Acid to Grapevine Resistance against the Biotrophic Oomycete *Plasmopara viticola*. *Front Plant Sci*. 7(565):1-7.

49. X Qiang, BB Zechmann, BUR Marco, K Karl-Heinz, SF Patrick. 2012. The Mutualistic Fungus Piriformospora indica Colonizes *Arabidopsis* Roots by Inducing an Endoplasmic Reticulum Stress.Triggered Caspase-Dependent Cell Death. *Plant cell*. 24:794-809.

50. SH Kim, C Kwon, JH Lee, T Chung. 2012. Genes for Plant Autophagy: Functions and Interactions. *Mol cell*. 34:413-423.

51. M Kei-ichiro, N Yukihiro, S Eiji, H Noriko, O Yoshiyuki, S Yukihisa, K Nozomu. 2012. Defects in IRE1 enhance cell death and fail to degrade

mRNAs encoding secretory pathway proteins in the *Arabidopsis* unfolded protein response. *PNAS*. 110(14):5713-5718.

52. C Ruberti, B Federica. 2014. Conserved and plant-unique strategies for overcoming endoplasmic reticulum stress. *Front Plant Sci*. 5(69):1-8.
53. SI Kwon, OK Park. 2008. Autophagy in Plants. *J Plant Bio*. 51(5):313-320.
54. GHM Sagor, C Pratima, DW Kim, T Berberich, S Kojima, M Niitsu, T Kusano. 2015. The polyamine spermine induces the unfolded protein response via the MAPK cascade in *Arabidopsis*. *Front Plant Sci*. 6(687):1-12.